European Train the Trainer Programme for Responders

Lecture 9

Hazard distances from hydrogen flames and fire fighting

LEVEL IV

Specialist officer

The information contained in this lecture is targeted at the level of specialist officer and above.

This topic is also available at levels I-III.

This lecture is part of a training material package with materials at levels I – IV : Firefighter, crew commander, incident commander and specialist officer. Please see the lecture introduction regarding competence and learning expectations

Note: these materials are the property of the HyResponder Consortium and should be acknowledged accordingly, the outputs of HyResponse have been used as a basis

Clean Hydrogen Partnership

Co-funded by the European Union

Disclaimer

Despite the care that was taken while preparing this document the following disclaimer applies: the information in this document is provided as is and no guarantee or warranty is given that the information is fit for any particular purpose. The user thereof employs the information at his/her sole risk and liability.

The document reflects only the authors' views. The FCH JU and the European Union are not liable for any use that may be made of the information contained therein.

Acknowledgments

This project has received funding from the Fuel Cells and Hydrogen 2 Joint Undertaking (now Clean Hydrogen Partnership) under Grant Agreement No 875089. This Joint Undertaking receives support from the European Union's Horizon 2020 Research and Innovation program, Hydrogen Europe and Hydrogen Europe Research.

Summary

This lecture is focused on ignited hydrogen releases (microflames, jet fires, fireballs). A useful terminology has been introduced at the start. Then a classification of different types of hydrogen fires is provided. Hydrogen jet fires (most typical for compressed gaseous storage) are discussed in detail. A significant part of the lecture is devoted to the evaluation of flame length and separation distances. Harm criteria for hydrogen technologies have been described. The effect of different factors on hydrogen flame length is discussed. The radiative heat fluxes and the flame lengths for jet fires of hydrogen, CNG and LPG was presented in this lecture. An overview of detection, and mitigation techniques for hydrogen fires is given. This information will be very useful not only for virtual reality and operational exercises but in decision making at a scene of an accident involving fires.

Keywords

Hydrogen fire, flame length, separation distance, radiation heat fluxes, detection, mitigation, extinction

Table of contents

Summary 3
Keywords 3
1. Target audience 6
1.1 Roll description: Specialist 6
1.2 Competence level: Specialist 6
1.3 Prior learning: Specialist 6
2. Introduction and objectives 6
3. Main terminology 7
4. Types of hydrogen fires and flames 9
4.1 Microflames 10
4.1.1 Hydrogen flames quenching 10
4.1.2 Leaky fittings 12
4.2 Hydrogen jet fires and flame length and hazard distances 13
4.2.1 The dimensional correlation 17
4.2.2 The dimensionless correlation 20
4.2.3 Determination of the flame length 25
4.2.4 The jet flame tip location 25
4.2.5 Hazard distances from hydrogen jet fire 27
4.3 Flame lengths and separation distances affected by different issues 31
4.3.1 The effect of jet attachment on flame length 31
4.3.2 The effect of nozzle size and shape on flame length 32
4.3.3 The effect of buoyancy on deterministic separation distances 34
4.3.4 The effect of barriers 34
5. Pipeline applications 35
6. Radiation heat fluxes from jet fires and fireballs 39
6.1 Radiation heat fluxes from jet fires 39
6.2 Hydrogen jet fires versus jet fires of common fuels 42
6.3 Hydrogen fireballs 43
6.4 Effect of delayed ignition on the pressure of hydrogen jet fires 43
6.5 Effect of various parameters on overpressure 44
6.5.1 The effect of an orifice diameter on overpressure 44
6.5.2 The effect of the ignition delay on overpressure 45
6.5.3 The effect of ignition source location on overpressure 46

7. Fire of FC vehicles 46
8. Detection, mitigation and extinction of hydrogen fires 53
8.1 Detection of hydrogen fires 53
8.1.1 UV detectors 55
8.1.2 IR detectors 56
8.1.3 Thermal detectors 56
8.1.4 Imaging systems 56
8.2 Mitigation of hydrogen fires 56
8.2.1 Control of the jet flow direction 56
8.2.2 Shielding or barriers 57
8.2.3 Reduction of flame length 57
8.2.4 Flashback and flame arrestors 58
8.2.5 Use of thermal insulation 59
8.3 Extinction of hydrogen fires 60
9. Flame length calculation of under-expanded jet fire 60
10. Relevant e-Laboratory tools 63
10.1 Calculation of flame length 63
10.2 Expanded and under-expanded jet 65
10.3 Calculation of hazard distance 66
Acknowledgement 67
References 67

1. Target audience

The information contained in this lecture is targeted at the level of specialist officer and above. The role description, competence level and learning expectations assumed at specialist officer level are described below.

1.1 Roll description: Specialist

Specialists assist Incident Commanders with advice and by directing and supervising technical operations that involve the use of knowledge, skills or equipment related to a specific risk or response activity. Typical incidents involve hazardous materials, transportation vehicles, climatic events, structural and other built environment failures and emergency response logistics.

1.2 Competence level: Specialist

A scientific, engineering and empirical foundation in the subject area with skills, extended by experience, to apply that information, knowledge in an interpreted and useful way to enable the Incident Commander and other first responders under the specialist's direction to respond effectively and safety to the emergency situation.

1.3 Prior learning: Specialist

EQF 5 Comprehensive, specialised, factual and theoretical knowledge within a field of work or study and an awareness of the boundaries of that knowledge. A comprehensive range of cognitive and practical skills required to develop creative solutions to abstract problems. Exercise management and supervision in contexts of work or study activities where there is unpredictable change; review and develop performance of self and others.

2. Introduction and objectives

Frequently, the term 'safety' is referred to as a 'non-technical' barrier to the emerging FCH technologies. However, there are several engineering challenges to be addressed before rolling out these technologies to the market. One of them is the reduction of hydrogen jet flame length from the current value of 10-15 m from FC vehicle on-board storage to allow the evacuation and rescue of passengers and their safeguarding by responders. Another important unresolved problem is to increase the fire resistance rating of on-board hydrogen storage tanks from 1-7 minutes (current value for type IV vessels) to allow the longer time for blow-down of tanks. This would prevent severe damage of civil structures such as garages during accidental hydrogen release. Additionally, it would exclude even a chance of large hydrogen-air clouds formation inside tunnels, which can lead to fatalities throughout the entire length of the tunnel in the case of fires. The higher fire resistance rating of hydrogen storage tanks would permit safe evacuation of civilians from an accident scene, providing life safety of passengers and responders [1].

Without a doubt, Responders will have to deal with incidents or accidents involving hydrogen flames because hydrogen fire is a typical scenario of many accidents. Knowledge of the

possible hydrogen flame length and related separation distances are of key importance for Responders. There will also be a thermal radiation from a fire, which can cause harm to humans and damage to structures, buildings, equipment, etc. at the distances beyond the flame length. Several factors that affect the extent of a jet fire and the associated radiative heat flux, including hydrogen storage pressure and a leak size, will be discussed in the present lecture. Methods of hydrogen fire detection, the techniques of hydrogen fires mitigation and extinction are considered in this lecture as well.

By the end of this lecture a Responder/a trainee will be able to:

- Distinguish between different types of hydrogen fires:
  from microflames to jet fires and fireballs,
- Evaluate hydrogen flame lengths with the aid of nomograms, dimensional and dimensionless correlations,
- Assess the average location of jet flame tip,
- Predict the determination separation distances to protect people and structures,
- Explain the effect of different factors on the flame length of jet fire: nozzle size and shape, jet attachment, buoyancy, barriers, or walls,
- Compare the flame lengths and heat fluxes of jet fires on hydrogen and other common fuels (CNG and LPG),
- Explain the pressure effects of hydrogen jet fires,
- Identify the main hydrogen fires detection methods,
- Recognise the mitigation techniques for hydrogen fires,
- Implement the hydrogen fires extinction practices,
- Appreciate the main safety challenges related to the current state of FCH technologies.

3. Main terminology

In order to fully understand hydrogen fires and other related phenomena (such as microflames, quenching, lift-off, blow-off and blow-out phenomena, thermal radiation, flame visibility, flame length and speed, impinging jet fires, etc.) it will be useful to learn a few definitions listed below. Please pay attention to the dimensionless numbers, which will be frequently used in the present and further lectures.

Blow-down is a process where the storage pressure decreases with time during a leak [1].

Blow-off is the flame extinguishment at a high velocity without a lift-off [2].

Blow-out is the flame extinguishment at high velocity with a lift-off [2].

Blow-out limit is a fuel flow velocity limit beyond which a lifted flame blows out [2].

Deflagration is the process following the weak ignition in a combustible mixture, which propagates at a subsonic speed into fresh, unburned mixture [3].

Detonation is the process, in which the combustion wave propagates with a supersonic velocity in the unreacted medium [3].

Drop-back is the reattachment to the nozzle of a lifted flame by a decrease of lift-off velocity [2].

Effective diameter is the jet diameter at the location where expansion down to 1 bar takes place, in an under-expanded jet [4].

Expanded jet is the jet with a pressure at the nozzle exit equal to atmospheric pressure [1].

Fire-resistance rating is a measure of time for which a passive fire protection system can withstand a standard fire resistance test [1].

Flame lift-off is the condition, in which the flame and a burner become separated.

Flame speed is the velocity of the flame with the respect to a fixed observer [3].

Flashpoint is the lowest temperature, at which the fuel produces enough vapours to form a flammable mixture with air at its surface [1].

Froude number (Fr) is the dimensionless number equal to the ratio of inertial to gravity force [1].

Hazard distance is a distance from the (source of) hazard to a determined (by physical or numerical modelling, or by a regulation) physical effect value (normally, thermal or pressure) that may lead to a harm condition (ranging from “no harm” to “max harm”) to people, equipment or environment.

Laminar burning velocity is the rate of flame propagation relative to the velocity of the unburned gas that is ahead of it, under stated conditions of composition, temperature, and pressure of the unburned gas [1].

Lift-off height is the height from the nozzle exit to the base of a lifted flame [2].

Lift-off velocity is the fuel flow velocity causing a flame to be detached from the nozzle [2].

Mach number (M) is the dimensionless number equal to the ratio of the local flow velocity to the local speed of sound [1].

Maximum Allowable Working Pressure (MAWP) is the maximum pressure, to which any component or portion of the pressure system can be subjected over the entire range of design temperatures [5].

Normal Temperature and Pressure (NTP) conditions are: temperature 293.15 K and pressure 101.325 kPa [1].

Non-premixed flame (often called a *diffusion flame*) is the flame, in which the oxidiser and the fuel are not mixed prior to reaching a flame front. During combustion oxidiser combines with a fuel by diffusion. The flame speed is limited by the rate of diffusion.

Overpressure is the pressure in a blast wave above the atmospheric pressure, or the pressure within a containment structure that exceeds the maximum allowable working pressure of the containment structure [5].

Premixed flame is the flame, in which the oxidiser has been mixed with the fuel prior to the reaching the flame front. Combustion of premixed fuel and oxidiser forms a thin flame front due to the reactants being readily available.

Quenching gap is the spark gap between two flat parallel-plate electrodes at which ignition of combustible fuel-air mixtures is suppressed. The quenching gap is the passage gap dimension requirement to prevent propagation of an open flame through a flammable fuel-air mixture that fills the passage [1].

Reynolds number (Re) is the dimensionless number that gives a measure of the ratio of inertial to viscous forces [1].

Hazard (or separation) distance is a minimum distance, which separates "specific targets (e.g. people, structures or equipment) from the consequences of potential accidents related to the operation a hydrogen facility" [6].

Under-expanded jet is the jet with a pressure at the nozzle exit above the atmospheric pressure [1].

*Visible flame length i*s the centerline distance from the tip of the nozzle to the flame end [2]. Visible, infrared (IR) and ultraviolet (UV) digital images are often used for the measurement of flame length and the measured flame lengths vary between different images [23].

4. Types of hydrogen fires and flames

Hydrogen may burn in different combustion modes, which include flash fire, jet fire, deflagration, detonation, etc. Hydrogen fires can range from microflames with the mass flow rate of 10^{-9} kg/s to the high mass flow rate flames (hundreds of kg/s). Hydrogen releases may burn as laminar diffusion or turbulent non-premixed flames depending on the Reynolds number (Re) at a leak exit. Flames can be buoyancy-controlled and momentum-dominated. Most hazardous hydrogen releases will be in a momentum-dominated regime. The jet fires can be, depending on the leak exit conditions, subsonic (the Mach number M<1), sonic and highly under-expanded supersonic. In the scenarios, where a failure of storage tank is possible with the immediate release of hydrogen into the surrounding atmosphere large size fireballs (tens of meters) can be formed. The presence of obstacles, surfaces and enclosures affect the jet flame significantly. A special case is the fires involving liquefied hydrogen (LH_2). Currently, there is a little knowledge available on LH_2 fires. There is a knowledge gap with an indication that condensation and solidification of oxygen (from the atmosphere) in the case of LH_2 leak/spill at certain condition may lead to explosive mixtures.

4.1 Microflames

The description of hydrogen microflames could be found in Section 3.13 in Lecture 2. The microflames are characterized by the low mass flow rate of hydrogen in the order of 10^{-9} kg/s (1 μg/s) in terms of subsonic laminar flows from cracks of the tanks.

4.1.1 Hydrogen flames quenching

There is generally a limited range of flow rates, for which a flame can be established on a burner nozzle. Below this range, the flow is said to be below the *quenching limit* [1]. Quenching of any flame occurs when the heat losses from flame are comparable with the heat generated through combustion, and thus the chemical reactions cannot be sustained. Hydrogen flames are difficult to quench. For example, premixed hydrogen-air combustion can be aggravated by heavy sprays of water due to induced turbulence and the ability of mixture to burn around the droplets. Hydrogen has the lowest quenching distance compared to other flammable gases.

The *quenching distance* is the maximum distance between two parallel plates that will extinguish a flame passing between them. The quenching distance decreases with the pressure and temperature increase. It also depends on the mixture composition [1]. The *quenching gap* is the spark gap between two flat parallel-plate electrodes, at which the ignition of combustible fuel-air mixtures is suppressed [1]. For the pre-mixed hydrogen-air mixtures two methods are often used:

- A circular tube, with the aid of which the quenching diameter is measured,
- A slot, through which the quenching distance is measured by referring to the width of the slot [10].

There is another term used to describe quenching of hydrogen flames: a *blow-off limit* corresponding to the flow rate reached, beyond which the flame *blows off* the nozzle [1]. Quenching and blow-off limits bound the leak flow rates that can support combustion.

The quenching and blow-off limits of different gases were measured by Kalghatgi [11], Matta et al. [12], Cheng et al. [13] for a variety of fuels including propane, methane and hydrogen on circular burners (Figure 1). As it follows from Figure 1 the quenching limits are nearly independent of diameter. Hydrogen has the lowest quenching limit and the highest blow-off limit.

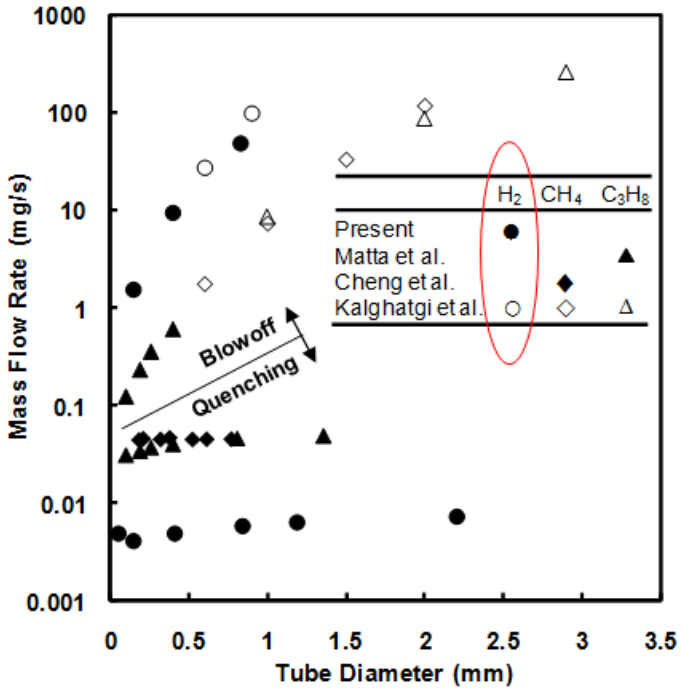

Figure 1. The quenching and blow-off limits of different fuels [1].

These studies showed that hydrogen mass flow rate blow-off limits are higher than those for methane and propane. For a given leak size, there is a range of mass flow rates where hydrogen is able to support a stable flame, but methane and propane would be blown off [1]. Butler et al. [14] studied the quenching limits for diffusion microflames controlled by the momentum. The quenching at such a small scale depends on the mass flow rate rather than the nozzle diameter. The experimental data defined the minimum mass flow rate needed for sustained ignition as 0.028 mg/s [14]. The diffusion flame below this value will be quenched. Figure 2 transposes the mass flow rate, necessary for sustained ignition, as a function of a burner diameter and upstream pressure, assuming choked flow, for three different fuels within a range of pressures. This graph confirms that quenching also depends on the pressure. Each line in Figure 2 begins at the minimum upstream pressure for choked flow and ends at the maximum pressure anticipated in FC vehicles. This plot predicts that for a given storage pressure, hydrogen is susceptible to leak flames for hole diameters that are smaller than those for methane or propane. Furthermore, at storage pressure of 69 MPa (690 bar) a hole with the diameter of just 0.4 μm is predicted to support a flame [1].

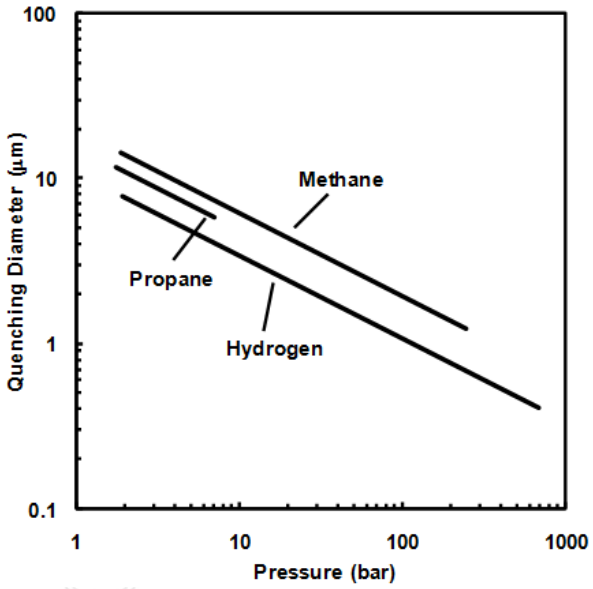

Figure 2. The quenching diameter as a function of upstream absolute pressure [14].

4.1.2 Leaky fittings

The compression fittings are often used for gases stored at high pressure. Figure 3 shows the measured mass flow rates for hydrogen, methane, and propane for a 6 mm leaky fitting in the vertical orientation [14]. The minimum flow rate necessary for sustained ignition is plotted versus pressure. For all three fuels limits are independent of pressure and hydrogen has the lowest values of quenching limits. Although hydrogen has the lowest mass flow rate necessary to sustain fittings micro-flames, propane has the lowest volumetric flow rate to sustain fittings micro-flames [3]. More details on leaky fitting can be found in [1].

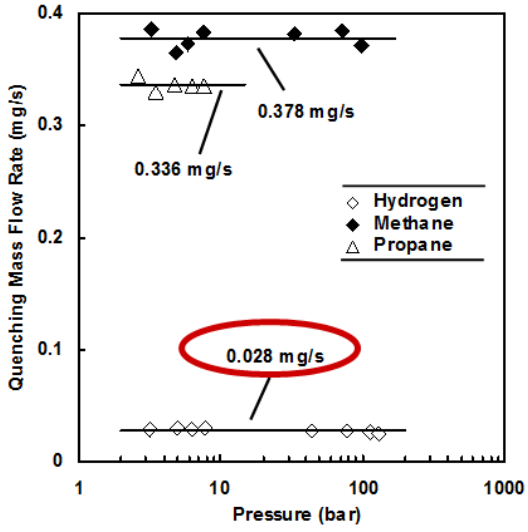

Figure 3. Quenching limits (mass flow rates) as function of upstream pressure in the vertical orientation of fittings [14].

Figure 4 shows images of flames from leaky fittings at quenching limits for hydrogen, methane and propane [15]. The top, middle and the bottom sets involve tube diameters of 3, 6 and 12 mm, respectively. Each fuel was flowing at the minimum flow rate needed to sustain flame.

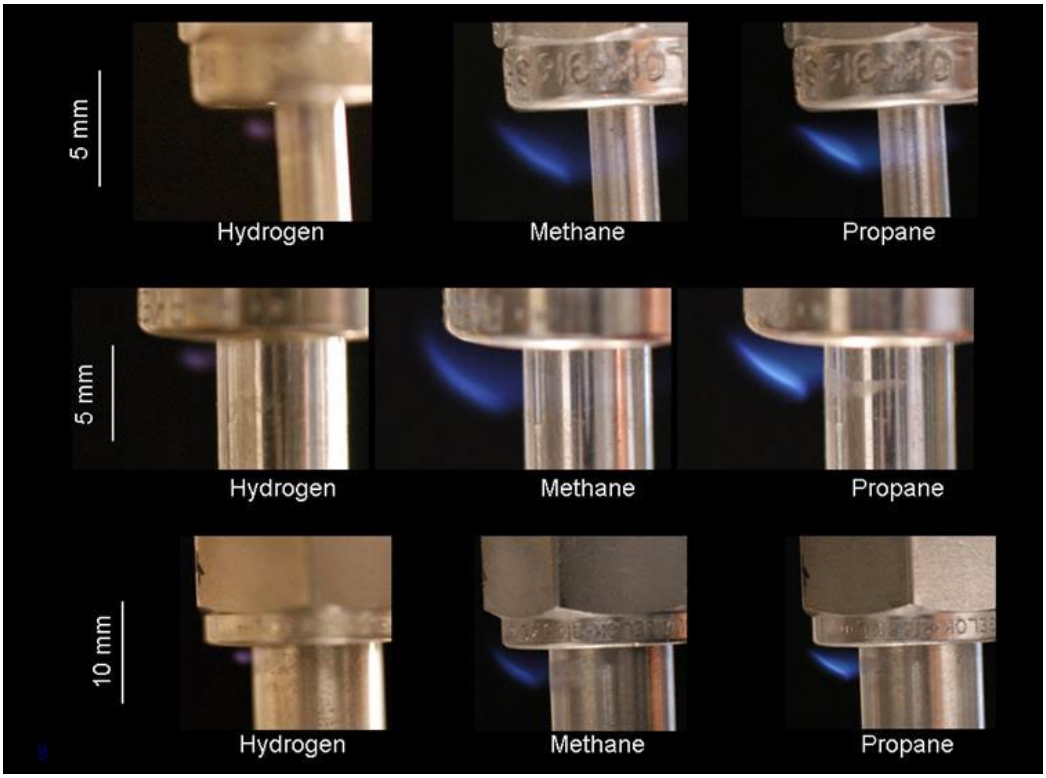

Figure 4. Images of flames at the quenching limits for hydrogen, methane and propane [15].

4.2 Hydrogen jet fires and flame length and hazard distances

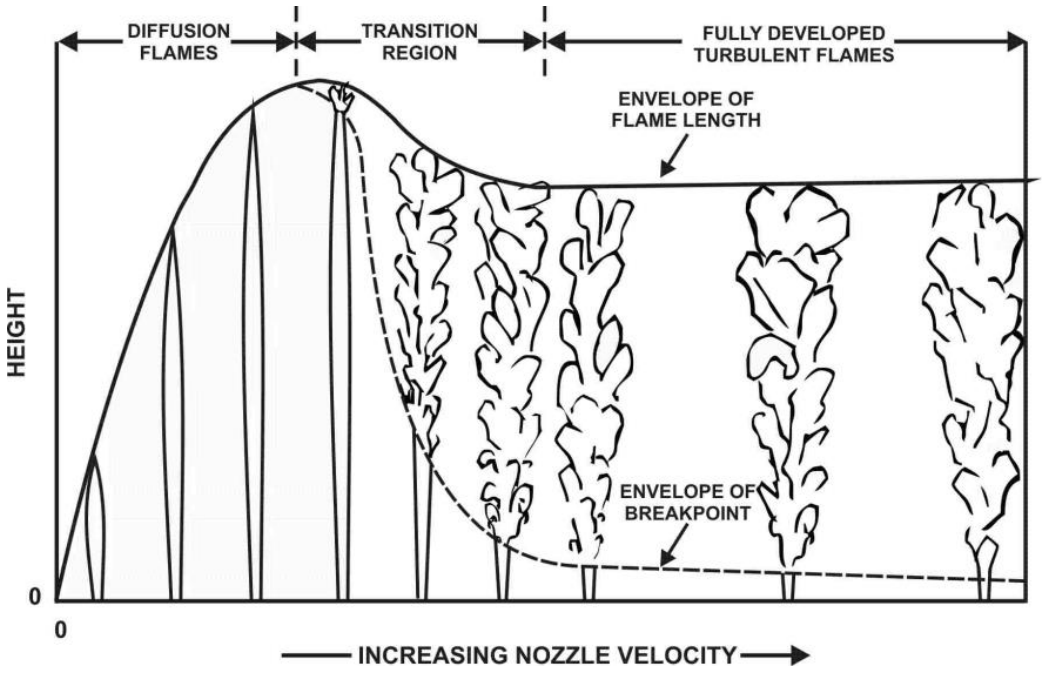

Figure 5. Progression from laminar diffusion to fully developed turbulent non-premixed flames [17].

Hottel and Hawthorne et al. [16, 17] concluded at their seminal study on expanded hydrogen flames that the flame length (L_F) is proportional to the nozzle diameter (D) only. The fuel gas flow rate was found to have no effect on the flame length as long as it is high enough to produce a fully developed turbulent flame (Figure 5).

Figure 5 shows the change of the flame height with the increase in nozzle velocity during transition from laminar diffusion to fully developed turbulent non-premixed flame as observed by Hawthorne et al. [16]. In the beginning the increase of nozzle velocity leads to the increase of flame length for laminar flames. Then, at some velocity the laminar flame height reaches its maximum and starts to decline as the flame becomes turbulent at its tip first. The transition from vertical laminar diffusion flame to turbulent flame starts to occur at Reynolds number of around Re = 2000 if the release of hydrogen into still air is considered.

It is not obvious that the conclusion made by Hawthorne et al. [16] on expanded jet fires regarding the independence of flame length on the nozzle velocity for turbulent jets can be extended to under-expanded jet fires. For instance, the turbulence and velocity fluctuation at the under-expanded jet axis downstream of the Mach disk is known to be quite high compared to sub-sonic flows [1]. This high level of turbulence in under-expanded jets has been confirmed recently by the application of the large eddy simulation (LES) technique by Brennan et al. [18] during processing the experimental data on large-scale hydrogen jet fires by Sandia National Laboratories.

Baev and Yasakov [19] theoretically showed that depending on the burner diameter D there will be a characteristic peak in the function $L_F/D = f(Re)$ mentioned by Hottel and Hawthorne [17], or there will be no peak for nozzles of the larger diameters (Figure 6).

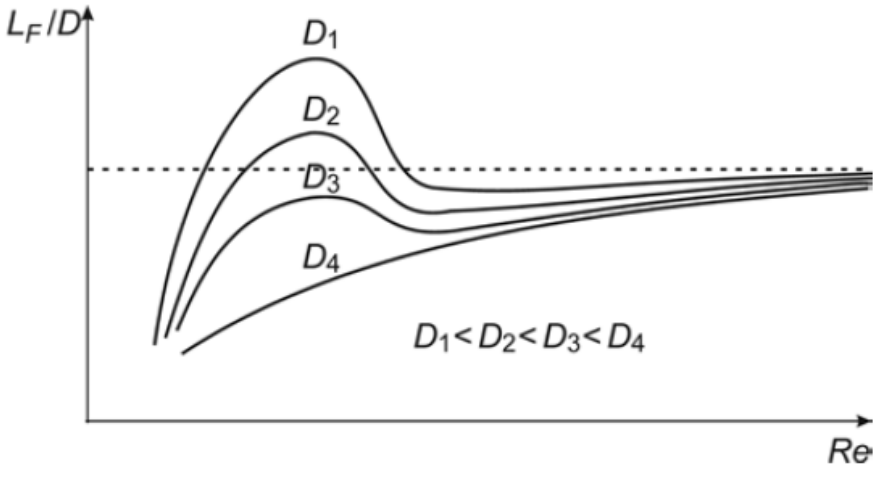

Figure 6. The theoretical flame length to diameter ratio (L_F/D) as a function of Reynolds number (Re) for different nozzle diameters D. The dotted horizontal line corresponds to a turbulent flame length limit L_t [19].

These theoretical predictions were confirmed by the experiments of Shevyakov and Komov [20] shown in Figure 7. The experimental dependence of L_F/D on Re up to Re = 20,000 is

presented for nine stainless steel tubular burners of diameter 1.45 - 51.7 mm. The burner length to diameter ratio was changing from 50 for smaller diameter burners to 10 for the largest one. The visual length of subsonic flames was measured in a darkened room. The hydrogen density of 0.0899 kg/m^3 and the temperature of 273 K were assumed in the nozzle exit during the processing of Shevyakov and Komov data [20] in our studies.

The experimental dependence of L_F/D on Re for smaller diameter (below 6 mm) burners has a characteristic peak predicted theoretically by Baev and Yasakov [19]. This peak height is decreasing with the increase of burner diameter in the area of transition from laminar to turbulent flow (Re < 2,300). Then L_F/D increases again with Re approaching a limit L_F/D = 220-230 at high Reynolds numbers. This experimental data is above a turbulent jet flame limit L_F/D = 190 measured by Baev and Yasakov [19]. It is worth noting that for the same Reynolds number L_F/D decreases with the diameter increase.

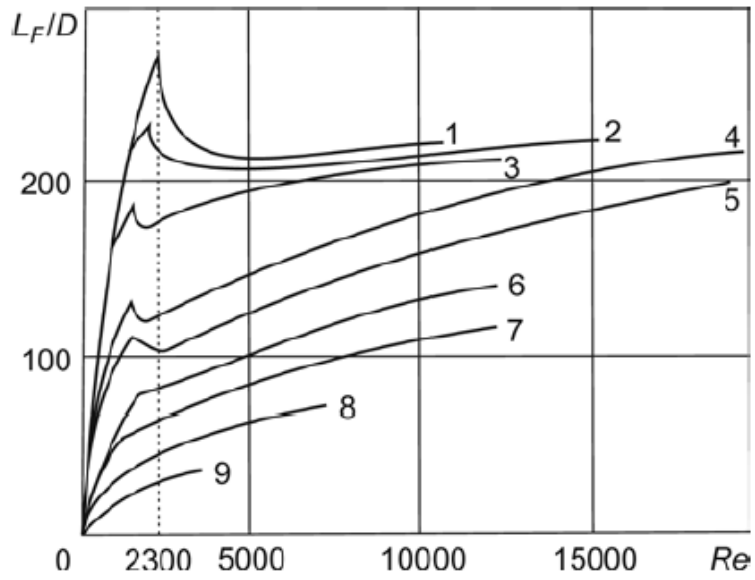

Figure 7. The experimental flame length to diameter ratio (L_F/D) as a function of Reynolds number (Re) for different nozzle diameters, D, mm: 1 – 1.45; 2 – 1.9; 3 – 2.9; 4 – 4.0; 5 – 6.0; 6 – 10.75; 7 – 15.5; 8 – 21; 9 – 51.7 [20].

Until recently all studies on hydrogen flames were limited to expanded jet flames or flames with high Reynolds number to conclude on functional dependence of jet flame length at Reynolds numbers characteristic for releases at pressures up to 100 MPa. While studies of Baev and Yasakov [19] and Shevyakov and Komov [20] answered the question on the existence of flame length peak during transition from laminar to turbulent flame, the question on the stabilisation or further increase of dimensionless flame length L_F/D with Reynolds number is yet to be answered [21]. A chronological and detailed review of hydrogen jet flame research can be found in Molkov [1].

Kalghatgi [22] published the experimental data of more than 70 tests with nozzle diameters in the range of 1.08 - 10.1 mm, both with subsonic and sonic hydrogen jet flames. Two important

conclusions can be drawn from this research. The conclusions are valid for both subsonic and sonic flows: 1) the flame length grows with the mass flow rate at a fixed pipe diameter D (D-constant), and 2) the flame length grows with the diameter at fixed mass flow rate $\dot{m}$ ($\dot{m}$ - constant). These conclusions put under doubt the generality of the statement by Hawthorne et al. [16] made by the analysis of expanded subsonic jets only, that jet flame length is proportional to nozzle diameter only and hydrogen flow rate is not a factor.

Dimensionless flame length correlations suggested by different authors are based on the use of the Froude number (Fr) only, in one form or another. Recently Fr-based correlations were expanded to high pressure hydrogen jet fires (under-expanded jets). The general idea of this technique is to correlate experimental data with the modified Fr number that is built on so-called *notional or effective nozzle diameter* instead of real nozzle diameter. However, the size of the notional nozzle diameter and the velocity in the notional nozzle are dependent on the theory applied, including several simplifying assumptions. To include the under-expanded jet fires into the dimensionless correlation, Schefer et al. [23] substituted actual nozzle diameter by effective (notional) nozzle diameter. In the subsequent study of Schefer et al. [24], the effective diameter was taken in the form $D_{eff} = D(\rho_N U_N/\rho_{eff} U_{eff})^{0.5}$ (where "N" denotes actual nozzle exit parameters and "*eff*" effective (notional) nozzle parameter) and is accepted here to build a correlation presented in Figure 8.

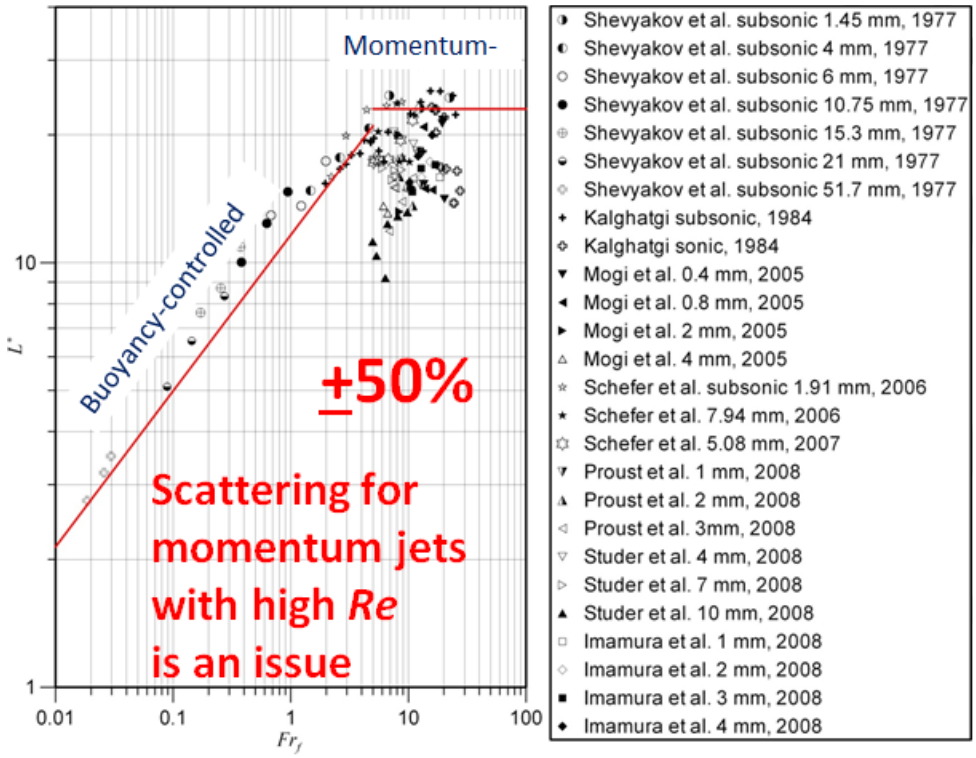

Figure 8. The Fr-based flame length correlation in coordinates used by Schefer et al. [24] with the extended range of experimental data on under-expanded jet fires.

Figure 8 demonstrates that flame length data is unacceptably scattered in the momentum-dominated area of the correlation with large Froude numbers, which are typical for leaks from

high pressure hydrogen equipment. It is clear that the simplification of flame length correlations to functional dependence on Froude number only, i.e. with ignoring the theoretically predicted and experimentally observed dependence on Reynolds and Mach numbers, does not make it work well when under-expanded jets are included [1].

4.2.1 The dimensional correlation

Figure 9 demonstrates that the use of new similarity group $(\dot{m}\cdot D)^{1/2}$ has essentially improved the convergence of the flame length data by Kalghatgi [22] and data published by other researchers for both subsonic and sonic jets. Figure 9 consolidates, in coordinates flame length L_F in m versus $(\dot{m}\cdot D)^{1/2}$ in $(kg\cdot m/s)^{1/2}$, ninety five experimental data points on hydrogen jet flame length in a wide range of pressures up to 90 MPa and nozzle diameters 0.4-10.1 mm [1].

The experimental data obtained by different research groups are collapsed onto the same curve, with the best fit line in Figure 9 being described by the following dimensional equation:

$$L_F = 76\cdot(\dot{m}\cdot D)^{0.347} \quad (1)$$

where D is the actual nozzle diameter, m; and $\dot{m}$ is the mass flow rate, kg/s. This equation requires knowledge of the actual leak diameter and the mass flow rate only. The mass flow rate can be calculated using any validated under-expanded jet theory. The advantage of this methodology is that it does not require substituting the actual nozzle diameter by the notional nozzle diameter. This excludes additional uncertainty in determination of parameters at notional nozzle exit related to particular assumptions of an under-expanded theory applied. The correlation is validated against subsonic, sonic, and supersonic hydrogen jet flames [1].

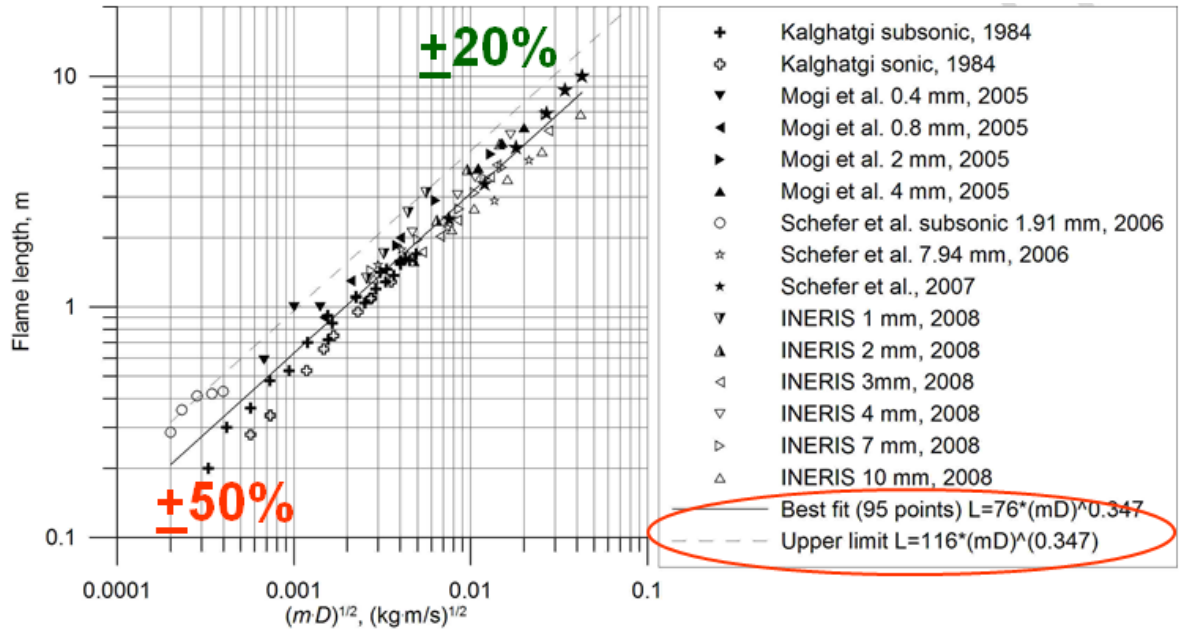

Figure 9. The dimensional correlation for hydrogen jet flame length [1].

The upper limit curve for the experimental flame lengths in Figure 9 (conservative estimate), is represented by the following equation:

$$L_F = 116 \cdot (\dot{m} \cdot D)^{0.347} \quad (2)$$

that yields 50% longer flame length compared to the best fit line described by the equation (1). The mass flow rate is by definition $\dot{m} \propto D^2$, therefore, correlations (1) and (2) give practically a linear dependence of the flame length on the nozzle diameter, $L_F \sim D$. In contrast, the correlation shows a weaker dependence of the flame length on the density and the velocity in the nozzle, $L_F \sim (\rho_N \cdot U_N)^{1/3}$.

The predictive capability of the dimensional correlation in Figure 9 is quite good for high debit jet fires (20%), and yet it is only about 50% for smaller debit flames, where the characteristic peak in the dependence $L_F/D = f(Re)$ for small diameters is one of possible reasons of the larger scattering in the experimental data. While the correlation is a convenient and reliable tool for hydrogen safety engineering at large mass flow rate leaks it is not shedding a light on the underlying the correlation physics, and it has a low predictive capability at smaller leaks [1].

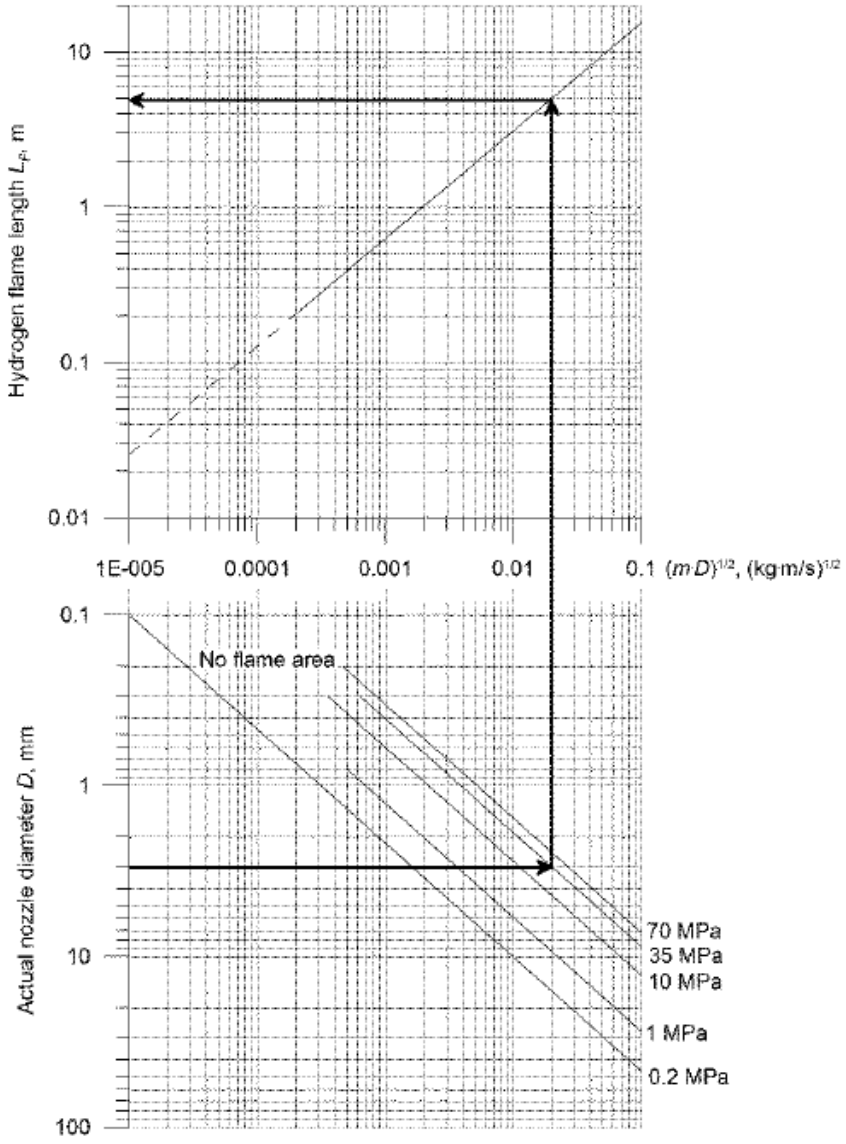

Figure 10. The nomogram for hydrogen jet flame length [1].

Figure 10 presents a nomogram designed to simplify the use of the dimensional correlation (1). The graphical estimation of jet flame length using the nomogram requires only two parameters of a leak, e.g. storage pressure and the actual diameter of the leak, which are usually available and do not require any calculations [1].

The nomogram on Figure 10 is derived from the best fit line of the dimensional flame length correlation shown in Figure 9. Please note that the conservative estimate of the flame length is 50% longer, and thus the value obtained from this nomogram should be multiplied by 1.5. The use of the nomogram for calculation of flame length is demonstrated in Figure 10 by thick lines with arrows. Firstly, an actual nozzle diameter of a leak, e.g. D = 3 mm in this example, and a storage pressure, e.g. 35 MPa, are chosen. Secondly, a horizontal line is drawn from the diameter axis at point 3 mm to the right until it intersects with the pressure line denoted as 35 MPa. Thirdly, a vertical line is drawn from the intersection point upward until the second intersection with the only line available in coordinates (L_F - $(\dot{m}\cdot D)^{1/2}$). Finally, to get a flame length a horizontal line is drawn from the second intersection to the left until the final intersection with the axis denoted "Hydrogen flame length L_F, m". In the example considered, the leak of hydrogen at pressure 35 MPa through the orifice of 3 mm diameter will result in the flame length of 5 m. The conservative estimate of the flame length as discussed above is 50% longer, i.e. 7.5 m [1].

The special feature of this nomogram is an area of 'No flame', which is observed for nozzle diameters 0.1 - 0.2 mm when flame blew-off although the spouting pressure was as high as 40 MPa. It should be noted that the nomogram does not account for the conditions when flow losses in a leakage pathway, which cannot be ignored. In such cases, a straightforward use of the nomogram gives a conservative result. A more accurate prediction of the flame length in equipment with essential friction and minor losses can be obtained if a method is available allowing calculation of the density in the nozzle exit affected by the losses. The nomogram can be used for a quick estimate of the hydrogen jet flame length. However, the use of the novel dimensionless flame correlation is recommended for more accurate calculation of the flame length.

Most of previously described and reviewed by Molkov [1] studies on hydrogen jet flames were performed with the extended jets, with the exception of recent studies, aiming to underpin safe introduction of hydrogen as a new energy carrier. The majority of leaks from high-pressure hydrogen equipment will be in the form of under-expanded jet (i.e., the jet with the pressure at the nozzle exit above the atmospheric pressure). This means that in order to predict accurately the parameters of hydrogen leaks at storage pressures above 10 MPa non-ideal behavior of hydrogen should be taken into consideration.

As mentioned earlier, the earlier notional nozzle model was developed by Schefer et al. [24]. Molkov and Saffers [25] had applied an alternative theory of under-expanded jet, which under-expanded jet conceptual scheme is shown in Figure 11. The parameters with sub-script 1

correspond to high-pressure storage where the assumption of zero flow velocity is made. The flow parameters at the entrance to the leak channel (i.e. nozzle) are referred to by sub-script 2, and at the nozzle exit – by sub-script 3. It is assumed that the flow is choked at the nozzle/channel exit and therefore the exit velocity is equal to the speed of sound. The notional nozzle exit, where parameters correspond to a fully expanded jet (pressure is equal to ambient), is referred to by sub-script 4. It is assumed that at the notional nozzle the flow velocity is uniform and locally sonic. It is also assumed that there is no air entrainment to the jet through the notional nozzle boundary (between 3 and 4) [25].

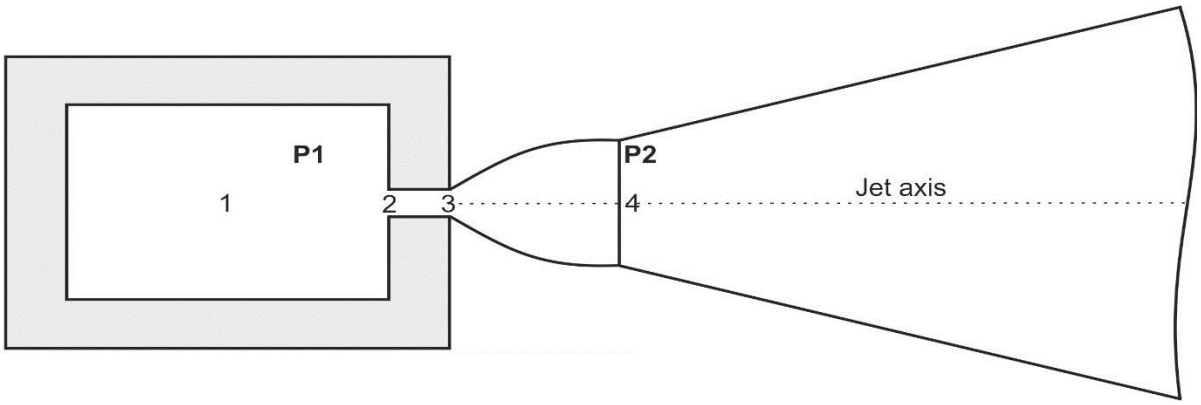

Figure 11. The under-expanded jet scheme [1].

1- High pressure vessel
2- Nozzle entrance
3- Nozzle exit (= notional nozzle entrance)
4- Notional (effective) nozzle exit (3-4: no entrainment).
The pressures are:
P1 - Storage pressure
P2 - Atmospheric pressure (after jet expansion).
In some cases, there can be essential minor and friction losses in the flow pathway 2-3 that cannot be neglected, e.g. the case of very narrow crack.

4.2.2 The dimensionless correlation

Practically all former flame length correlations are *Fr*-based and built on the experimental data for sub-sonic buoyant jet/plume fires with a limited number of momentum-controlled jet fires at moderate pressures. *Fr*-based "correlation" is lacking physical commonality when a large number of experimental data on under-expanded jet fires are included (all in the momentum-dominated regime) [1].

Theoretical and experimental results indicate that the flame length must be a function of not only the Froude number (*Fr*) but also the Reynolds (*Re*) number and the Mach (*M*) number [1]. The dimensional correlations similar to those depicted in Figure 9 are convenient engineering tools, yet they do not make a distinction between different jet fire regimes. This section of the lecture aims to advance the understanding of hydrogen jet flame behavior. A dimensionless

correlation for non-premixed flames that will differentiate between traditional buoyancy-controlled and momentum-dominated jet flames, as well as between expanded and under-expanded jet fires will be discussed below.

The dimensional correlation (1) can be approximated as $L_F \propto (\dot{m} \cdot D)^{1/3}$. The mass flow rate is by definition $\dot{m} \propto D^2$. Thus, a conclusion can be drawn after substitution of $\dot{m} \propto D^2$ into the above relationship for L_F that the dimensionless flame length, L_F/D, does not depend explicitly on the diameter, D. This is a basic hypothesis behind the development of a novel dimensionless correlation for the jet flame length, which is supported by the experimental data analysis. The only dependence of the dimensionless flame length, L_F/D, is then on the "residual" parameters in the mass flow rate (i.e. density ρ_N and velocity U_N at the nozzle exit), which are assumed uniform for the simplicity [25].

The density and velocity can be normalized as ρ_N/ρ_S and U_N/C_N respectively, where C_N is the speed of sound at conditions of gas in the nozzle and ρ_S is the density of the surrounding gas (air). In assumption of the kinetic energy flux in the nozzle exit to be a conserved scalar of the process a relation between the density and the velocity in the dimensional group can be suggested as $(\rho_N/\rho_S)(U_N/C_N)^3$.

Figure 12 presents a novel dimensionless hydrogen flame length correlation. In this correlation the experimental data on flame length are normalized by the actual (not notional) nozzle diameter, and are correlated with the product of the dimensionless density ratio ρ_N/ρ_S and the Mach number (ratio of the flow velocity to the speed of sound at the actual nozzle exit) to the power of three $M^3=(U_N/C_N)^3$.

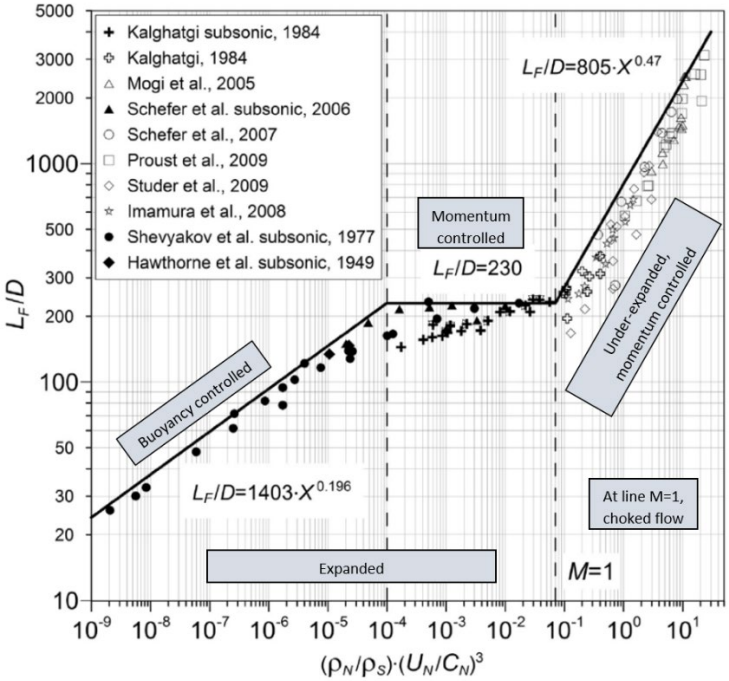

Figure 12. The dimensionless correlation for hydrogen jet flames (in formulas "X" denotes the similarity group $(\rho_N/\rho_S)\cdot(U_N/C_N)^3$).

One of the advantages of this correlation is the absence of parameters at the notional nozzle exit. The parameters needed to predict the flame length are those at the actual nozzle exit only: diameter, hydrogen density and flow velocity, the speed of sound at pressure and temperature at the nozzle exit. There is lesser uncertainty in calculation of flow parameters in the actual nozzle exit compared to uncertainties at the notional nozzle. Indeed, it is well known that there is a strong non-uniformity of velocity immediately downstream of the Mach disk that deviates from the common for all under-expanded jet theories assumption of uniform velocity at the notional nozzle exit. By this fact, the developed methodology excludes from consideration the questionable issue of use of flow parameters at the notional nozzle exit [1].

The correlation covers the whole spectrum of hydrogen reacting leaks, including laminar and turbulent flames, buoyancy- and momentum-controlled fires, expanded (subsonic and sonic) and under-expanded (sonic and supersonic) jet flames in the range of leak source pressures from 0.1 to 90 MPa and leak diameters from 0.4 to 51.7 mm.

The dimensionless group derived for correlating the dimensionless flame length can be rewritten in terms of *Re* and *Fr* numbers as follows:

$$\frac{\rho_N}{\rho_S}\left(\frac{U_N}{C_S}\right)^3 = \frac{g}{\rho_S}\frac{\mu_N}{C_N^3}\cdot Re\cdot Fr \tag{3}$$

where the viscosity was calculated as $\mu_N = \mu_{293}\cdot\left[(293+K_{Suth})/(T_N+K_{Suth})\right]\cdot(T_N/293)^{3/2}$ (Sutherland constant for hydrogen was taken as K_{Suth} = 72 K and the dynamic viscosity as μ_{293} =8.76×10^{-6} Pa·s), and *Re* and *Fr* are determined by parameters of hydrogen flow in the actual nozzle exit from the following equations:

$$Re = \frac{\rho_N\cdot d_N\cdot U_N}{\mu_N} \tag{4}$$

$$Fr = \frac{U_N^2}{d_N\cdot g} \tag{5}$$

The form of the dimensionless group in the left-hand side of the equation (3) suggests that for subsonic flows, when Mach number $M < 1$ and the density ratio ρ_N/ρ_S is a constant for expanded jets (in assumption of constant temperature in the nozzle), the dimensionless flame length depends on the nozzle Mach number only. For choked flows in the nozzle exit (M = 1) the dimensionless flame length depends only on the hydrogen density in the nozzle exit ρ_N. The density increases with the increase of storage pressure and the decrease of hydrogen temperature.

The form of the right-hand side of the equation (3) indicates that at a constant temperature of hydrogen in the nozzle exit (that provides the constancy of the speed of sound C_N) the dimensionless flame length depends on both *Fr* and *Re* numbers. This is contrary to the former correlations built on *Fr* number only.

There are three distinct parts in the novel dimensionless correlation in Figure 12 (from the left to the right): traditional buoyancy-controlled, traditional momentum-dominated "plateau" (expanded jets), and a new momentum-dominated under-expanded jet fire "slope". These three parts can be approximated by the following equations (conservative curves) respectively:

$$L_F/D = 1403 \cdot X^{0.196}, \text{ for } X = \frac{\rho_N}{\rho_S}\left(\frac{U_N}{C_N}\right)^3 < 0.0001 \quad (6a)$$

$$L_F/D = 230, \quad \text{for } 0.0001 < X = \frac{\rho_N}{\rho_S}\left(\frac{U_N}{C_N}\right)^3 < 0.07 \quad (6b)$$

$$L_F/D = 805 \cdot X^{0.47}, \quad \text{for } X = \frac{\rho_N}{\rho_S}\left(\frac{U_N}{C_N}\right)^3 > 0.07 \quad (6c)$$

There is a saturation of L_F/D for expanded jet fires as the flow velocity in the actual nozzle exit is approaching the speed of sound. The value of this saturation limit $L_F/D = 230$ reproduces results of a number of previous studies with expanded jets, though in the new coordinates. However, there is no saturation of the dimensionless flame length for choked under-expanded jet flames. Reported in recent under-expanded jet fire experiments Proust et al. [26] values up to $L_F/D = 3000$ are significantly higher compared to the limit $L_F/D = 230$ for expanded jets.

The shape of the correlation in Figure 12 has a physical meaning based on the knowledge of jet flame behavior. For example, the dimensionless flame length, L_F/D, increases for laminar and transitional flames (usually identified as "buoyancy-controlled" regime, low *Re*), then it is practically constant for transitional and fully developed turbulent expanded flames (traditionally named as "momentum-dominated" regime, moderate *Re*), and it increases again for under-expanded jets (momentum-controlled under-expanded jet regime, high *Re*). The growth of dimensionless flame length in the under-expanded regime is due to the fact that the dimensionless flame length is defined through the actual nozzle exit diameter, which is a constant, while in reality the under-expanded jet expands to atmospheric pressure at the notional nozzle exit, the flame length increases with the increase of density in the nozzle [1].

Figure 13 demonstrates changes of dimensionless numbers *Re, Fr, M*, for the experiments used for the development of the dimensionless correlation, as a function of the similarity group $(\rho_N/\rho_S)(U_N/C_N)^3$. The analysis of *Re, Fr, M* functional dependence on the similarity group shows that for under-expanded jets the dimensionless flame length growth depends practically on *Re* only. Indeed, the nozzle flow for under-expanded jets is choked (i.e. local $M = 1$), and the nozzle *Fr* number is practically constant also (the scattering of *Fr* is due to the difference in nozzle diameters of about one order of magnitude).

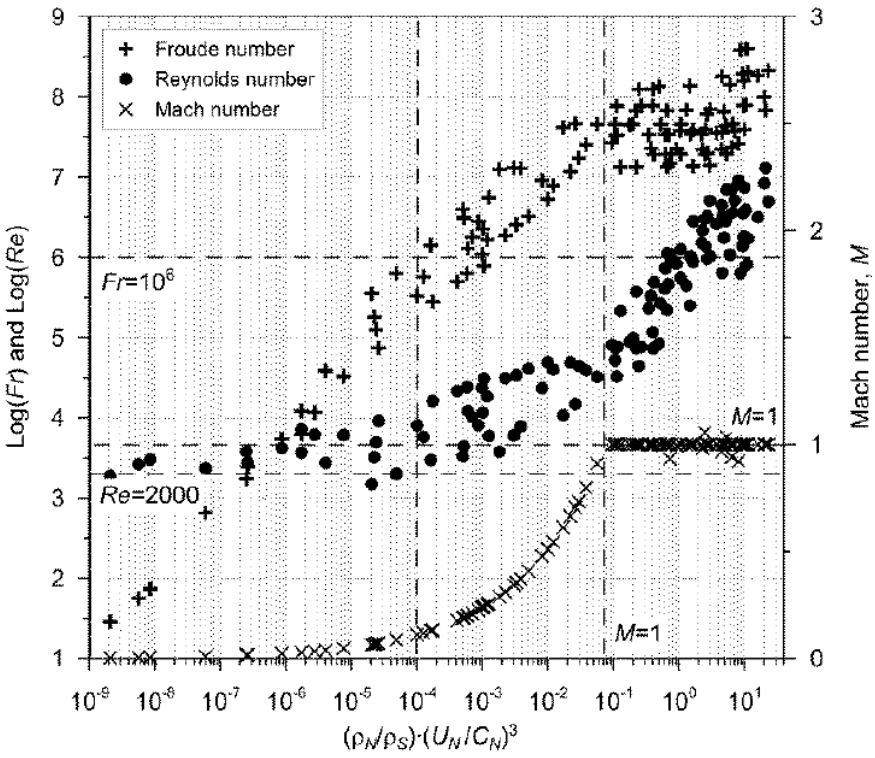

Figure 13. Dimensionless numbers *Re, Fr, M* as a function of the similarity group $(\rho_N/\rho_S)(U_N/C_N)^3$ for the experiments used to build the dimensionless correlation.

There are five dashed lines in Figure 13. Line $Re = 2000$ indicates the start of transition from laminar to turbulent nozzle flow. Close to (or immediately above) this line there are experimental points representing laminar jet flames and jet flames in the transitional regime. Horizontal line $M = 1$ indicates a choked flow limit. Subsonic expanded jets have $M < 1$ and sonic and supersonic (the last is relevant to notional nozzle flows only) under-expanded jets have $M = 1$ in the nozzle exit. There is some scattering of data around $M = 1$ due to measurements and data processing errors. Horizontal line $Fr = 10^6$ is an approximate division between buoyancy-controlled ($Fr < 10^6$) and momentum-dominated ($Fr > 10^6$) jets established previously for expanded jets. A vertical line at a value of the similarity group $(\rho_N/\rho_S)(U_N/C_N)^3 = 10^{-4}$ conditionally separates buoyant jet fires (to the left from the line) and momentum jet fires (to the right from the line). Finally, a vertical line denoted $M = 1$ divides subsonic (to the left) and sonic or chocked in the nozzle exit jets (to the right) [1].

In log-log coordinates in Figure 13 the *Fr* number increases linearly with the similarity group $(\rho_N/\rho_S)(U_N/C_N)^3$ for expanded jet fires. There is practically no change of *Fr* for under-expanded jets in this new system of coordinates (scattering is mainly due to difference in nozzle sizes). There is a slight growth of *Re* with the similarity group for buoyant jets, moderate increase in traditional momentum-dominated area, and comparatively steep growth of *Re* number in the area of under-expanded jet fires that are all momentum-dominated [1].

4.2.3 Determination of the flame length

The information discussed below will provide the guidance on how to evaluate the flame length based on the dimensionless correlation. In Figure 12, Y axis corresponds to the ratio, L_F/D, where L_F (m) is the flame length, D (m) is the nozzle diameter; X axis corresponds to $(\rho_N/\rho_S)(U_N/C_N)^3$, where ρ_N (kg/m^3) is the density of hydrogen at the nozzle exit, which can be found in the same way as with similarity law for unignited jets (see the Lecture 7 – Unignited hydrogen releases outdoors and their mitigation). It is equal to 0.0838 kg/m^3 at NTP for sub-sonic and expanded sonic jets. If the jet is under-expanded, then the density is calculated by the *under-expanded jet theory* developed by UU. ρ_S is the density of the surroundings (air), which equals to 1.205 kg/m^3. C_N is the speed of sound in hydrogen at the nozzle exit, which can be calculated using the equation (7):

$$C_N = \sqrt{\gamma \frac{P}{\rho}} = \sqrt{\gamma \frac{RT}{M}} \tag{7}$$

where γ is the ratio of specific heats at constant pressure and constant volume, M is the molecular mass, U_N is the velocity of the hydrogen at the jet exit. $U_N = C_N$ for sonic and supersonic jets, for sub-sonic jets the velocity is calculated as:

$$U_N = \sqrt{2 \frac{\Delta P}{\rho}} \tag{8}$$

4.2.4 The jet flame tip location

The experimental data demonstrated that the longest, and thus the most hazardous, flames are associated with under-expanded jets [1]. This is important to underline that all experimental data on the under-expanded jet fires are in the momentum-dominated regime (high value of Froude number *Fr*). This is due to high velocity of chocked flows and comparatively small diameters of piping for equipment working at pressures up to 100 MPa. The similarity law for axial concentration decay in round unignited expanded and under-expanded momentum-dominated jets discussed in Lecture 7 – Unignited hydrogen releases outdoors and their mitigation is shown in the equation (9):

$$C_{ax}^m = 5.4 \sqrt{\frac{\rho_N}{\rho_S}} \frac{D}{x} \tag{9}$$

where C_{ax}^m is the axial mass fraction of hydrogen in the jet at the distance x from the nozzle, ρ_S is the density of the surrounding gas, i.e. air (1.205 kg/m^3 at NTP), D is the actual nozzle diameter exit, ρ_N is hydrogen density in the nozzle exit.

The similarity law allows deriving a functional dependence $x/D=f(p)$ between the dimensionless distance from the leak source x/D and the storage pressure p (that is unambiguously related with the density at the nozzle exit, ρ_N) for any particular mass fraction of hydrogen on the jet axis, C_{ax} [1].

Figure 14 presents a correlation between the location of hydrogen jet flame tip (i.e. flame length) and the location of hydrogen concentration in unignited jet originating from the same leak source and the storage pressure, p. The points in Figure 14 represent the dimensionless experimental flame length, L_F/D. The diagonal curves in the graph correspond to the dimensionless distance x/D to the location of particular axial hydrogen concentration, C_{ax}, as a function of the density in the nozzle exit, ρ_N, (recalculated to the storage pressure, p in atmospheres, in Figure 14) and calculated using the similarity law (9).

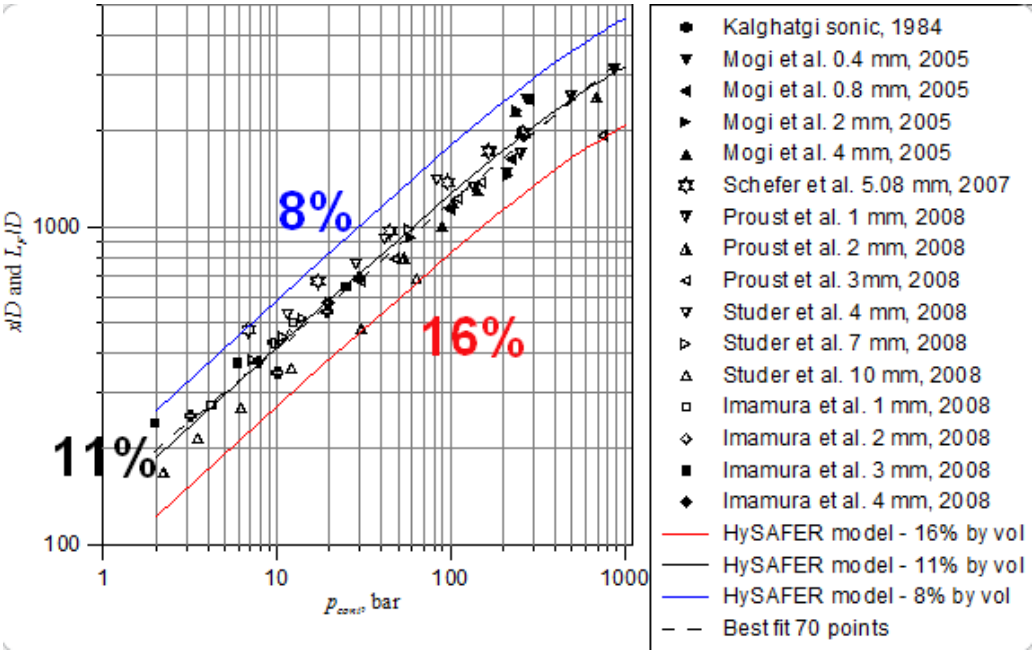

Figure 14. The correlation between the dimensionless flame length, L_F/D, and the distance to a particular concentration in a non-reacting jet, x/D, from the same leak source for different storage pressures, p.

The conclusion can be drawn from Figure 14 that, for momentum-controlled round jet fires, the flame tip is located where the axial concentration of hydrogen in an unignited jet, from the same leak source, is in the interval between 8 vol. % and 16 vol. %, depending on experimental conditions. The best fit line of 70 experimental points for hydrogen flame length of momentum-dominated jet fires is close to 11 vol. % of hydrogen in air in an unignited jet. These concentrations (8% to 16%) are far below the stoichiometric concentration of 29.5 vol. % of hydrogen in air. The distances to these concentrations from the nozzle are longer by 2.2 times (16%) to 4.7 times (8%) than the distance to the axial concentration of 29.5% (stoichiometric hydrogen-air mixture). This obviously could have serious safety and economic implications [1].

The nomogram developed originally for unignited releases, e.g. the hazard distance to the concentration in unignited jet 4 vol. %, can be applied now to graphically evaluate the flame length (Figure 15). This is due to the knowledge that flame tip location is in the place where the concentration in unignited jet from the same source decays to 8-16 vol. % of hydrogen with

the average flame length located where unignited release concentration decays to 11 vol. % [21].

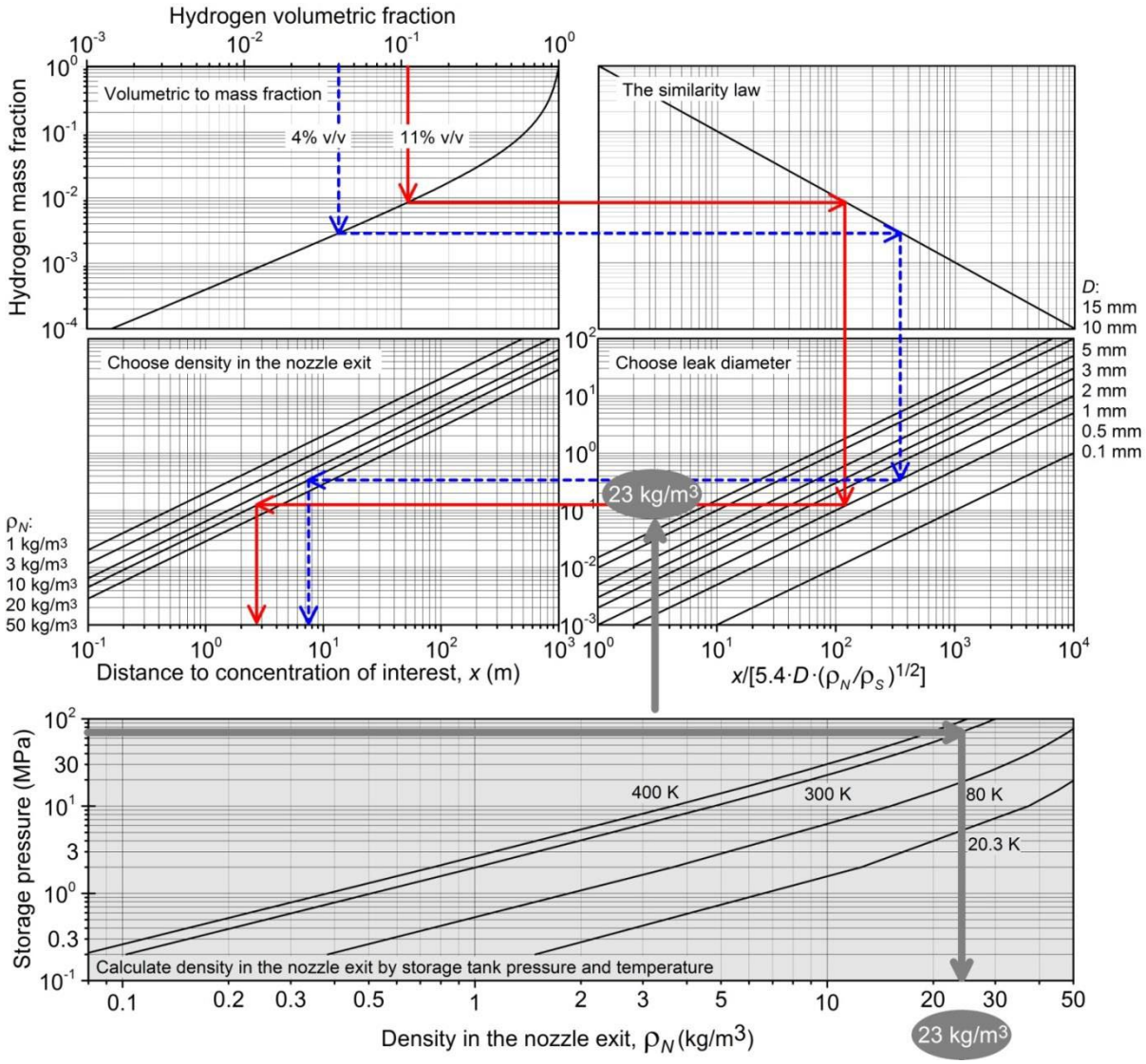

Figure 15. The nomogram for graphical evaluation of the flame length by concentration decay in unignited jet from the same source to 11 vol. %.

The example with 11 vol. % of hydrogen (red arrowed lines in Figure 15) shows that the average flame length for 1 mm diameter leak from storage at pressure of 70 MPa and temperature of 300 K would give flame length of about 2.7 m [21].

4.2.5 Hazard distances from hydrogen jet fire

The knowledge of the flame length is important for the assessment of the hazard and separation distances.

As per draft ISO TC197 definition, *hazard* distance is a distance from the (source of) hazard to a determined (by physical or numerical modelling, or by a regulation) physical effect value (normally, thermal or pressure) that may lead to a harm condition (ranging from “no harm” to “max harm”) to people, equipment or environment.

The separation distance (SD) is also known as a safety distance or setback distance is a subject of international debate.

According to LaChance (2009) SD is "a minimum distance, which separates specific targets (e.g. people, structures or equipment) from the consequences of potential accidents related to the operation a hydrogen facility" [27].

European Industrial Gases Association [28] defines SD as "a minimum separation between a hazard source and an object (human, equipment or environment) which will mitigate the effect of a likely foreseeable incident and prevent a minor incident escalating into a larger incident".

The following factors affect the SDs:

- the nature of the hazard,
- the operating conditions and the design of the analysed equipment/facility,
- the type of target/object (people, structures, equipment)
- the environment between the latter and the source of hazard. In this way, the harm potential for people or structures can be evaluated and compared with the harm criteria.

Different engineering tools to calculate hydrogen jet flame length are developed and described above. They include the dimensional and dimensionless correlations for the jet flame length, as well as the methodology to calculate hydrogen axial concentration decay to 11 vol. % in an unignited jet to evaluate the flame tip location (flame length). However, the question about separation distances from a leak source based on a comparative analysis of hazards from unignited jet and jet fire is not yet finalised [1].

Before calculating the hazard distance, it is necessary to consider what you would like to protect against. In the case of free fires this would be the temperature and the heat flux (in the case of enclosure fires - asphyxiation and overpressure may also be relevant). For people direct flame contact as a result of a jet fire is generally assumed to result in third degree burns. For people not in the flame, there is still potential for exposure to high radiation heat fluxes.

Harm criteria for people can be expressed in terms of injury or death [27]. It is possible to use a "no harm" criterion, which limits the level of acceptable consequences, to a low enough level that no injury would occur. Temperature 70 °C is taken as "no harm" criterion in this study. The exposures to flames, hot air or radiant heat fluxes can result in first-, second-, or third-degree burns. The resulting level of harm is dependent upon several factors: the amount and location of exposed skin, the person's age, the exposure time, the speed and type of medical treatment, etc. [1].

British standard [29] recommends 115 °C as a threshold for pain from an elevated air temperature for an exposure that lasts longer than 5 minutes. This is in line with the previously published classification by DNV [30] of elevated temperature effects on occupants: below 70 °C, no fatal issue in a closed space except uncomfortable situation; between 70°C and 150°C,

the impact is dominated by difficulties to breath; above 150°C, skin burns occur in less than 5 minutes and this is a limiting temperature for escape [30]. Time to incapacitation in minutes as a function of air temperature (°C) can be estimated by the following equations recommended by DNV [30] and BSI [31], respectively:

$$t_{inc} = 5.33 \times 10^{8} T_{air}^{-3.66} \tag{10}$$

$$t_{inc} = 5.0 \times 10^{7} T_{air}^{-3.4} \tag{11}$$

For temperature 115 °C, equation (10) gives the incapacitation time 5 minutes of exposure and equation (11) gives 15 minutes. Temperature 115 °C is assumed here as the acceptance criteria for pain limit in hot air when considering an escape from an elevated temperature gas flow generated by a hydrogen jet fire. More details on physiological response of humans to air at elevated temperature are discussed in the Lecture 6 - Harm criteria for people and property.

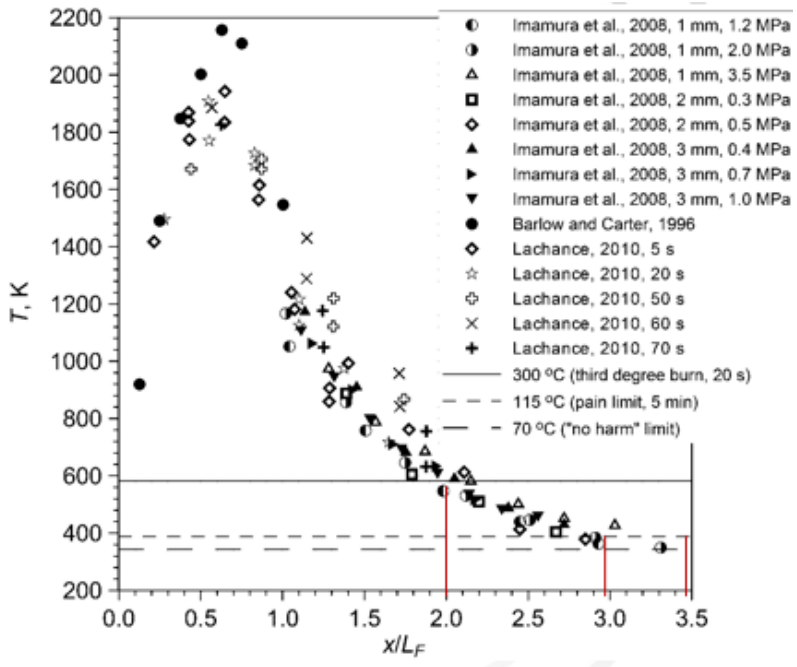

Figure 16. Measured axial temperature as a function of distance expressed in flame calibres, and three criteria for jet fire effects (horizontal lines).

Figure 16 shows measured axial temperature of hydrogen flame [27, 32, 33] as a function of distance from the nozzle, x, normalised by the flame length, L_F. Three accepted criteria are presented by horizontal lines:

- 70 °C - “no harm” limit,
- 115 °C - pain limit for 5 min exposure,
- 309 °C - third degree burns for a 20 s exposure (“death” limit).

A comparison between the axial temperature profile and named criteria provides the hazard distances:

- $x = 3.5L_F$ for "no harm" separation (70 °C),
- $x = 3L_F$ for pain limit (115 °C, 5 min),
- $x = 2L_F$ for third degree burns (309 °C, 20 s).

A comparison of three hazard distances for momentum-controlled jet fire and a hazard distance for momentum-dominated unignited release (distance to the lower flammability limit, LFL, of 4 vol. % of hydrogen in air) for the same leak source was carried out. It is demonstrated above that the statistically averaged flame length is equal to the distance from the nozzle to an axial location where hydrogen concentration decays to 11 vol. % in unignited jet (data are scattered from 8 to 16 vol. %).

The similarity law (9) for concentration decay in unignited momentum-controlled jets requires the use of hydrogen mass fraction and not volumetric fraction as mistakenly applied in some published work. The mass fraction (C_M) can be calculated by the volumetric (mole) fraction (C_V) by equation $1/C_M=1+(1/C_V -1)M_S/M_N$, where M_S and M_N are the molecular mass of surrounding gas and nozzle gas respectively. For air composition of 21 vol. % of oxygen and 79 vol. % of nitrogen the mass fraction of hydrogen $C_{ax} = 0.002881$ corresponds to 4 vol. % of hydrogen in air, 0.008498 corresponds to 11 vol. % of hydrogen ($C_{ax} = 0.005994$ – to 8 vol. %, $C_{ax} = 0.013037$ – to 16 vol. %), and mass fraction of hydrogen in stoichiometric mixture (29.5 H_2 vol. %) is $C_{ax} = 0.0282$ [1].

The ratio of distances from the nozzle to axial concentration 11 H_2 vol. % (correct flame tip location) and to 29.5 H_2 vol. % (incorrect location of the flame tip suggested in some studies) can be estimated by dividing the similarity laws (9) for these two concentrations by each other (in assumption that the similarity law is applicable up to concentrations as high as stoichiometric), i.e. $x_{11\%}/x_{29.5\%} = C_{ax(29.5\%)}/C_{ax(11\%)} = 0.0282/0.008498 = 3.3$. This increases calculated flame length by an order of magnitude compared to that based on the previous incorrect knowledge (attributing flame length tip location to location of 29.5 H_2 vol. % in unignited jet from the same source) [1].

The ratio of distances to LFL of 4 vol. % and to the averaged flame tip location of 11 vol. % is (it has to be stressed that flame length is not equal to hazard distance from the flame source): $x_{4\%}/x_{11\%} = 0.008498/0.002881 = 2.95$ (LFL distance to longest flame length ratio is $x_{4\%}/x_{8\%} = 2.08$, and LFL to shortest flame ratio is $x_{4\%}/x_{16\%} = 4.53$). Thus, ratios of the hazard distance to LFL (unignited jet) to three hazard distances based on the choice of harm criteria from reacting hydrogen jet are (for average flame tip location at concentration in unignited jet of 11 vol. %):

- $x_{4\%}/x_{T=70\,°C} = x_{4\%}/(3.5 \cdot x_{11\%}) = 2.95/3.5 = 0.84$,
- $x_{4\%}/x_{T=115\,°C} = 2.95/3 = 0.98$,
- $x_{4\%}/x_{T=309\,°C} = 2.95/2 = 1.48$.

However, in the conservative case of the flame tip location at the concentration of 8 H_2 vol. % in unignited jet, these three ratios will change to the following values respectively:

- $x_{4\%}/x_{T=70\,°C} = x_{4\%}/(3.5 \cdot x_{8\%})$ = 0.005994/0.002881/3.5 = 2.08/3.5 = 0.59,
- $x_{4\%}/x_{T=115\,°C}$ = 2.08/3 = 0.69,
- $x_{4\%}/x_{T=309\,°C}$ = 2.08/2=1.04.

As a result, an "unexpected" conclusion can be drawn from the performed analysis that in the conservative case all three hazard distances for reacting release (jet fire) are either longer or equal to the hazard distance based on the LFL (unignited release). In particular, the hazard distance from a hydrogen leak source to a location with axial concentration equal to the LFL, e.g. to prevent ingress of flammable mixture into a ventilation system of a building, is practically equal to the "death" separation distance for reacting release (exposure to 309 °C during 20 s). Two other hazard distances for jet fires ("no harm" and "pain" limits) are longer than the hazard distance to LFL (unignited release) [1].

The revealed "longest" location of the hydrogen jet flame tip at axial distances from the nozzle corresponding to 8 vol. % of hydrogen in unignited jet is a physically sound result. Indeed, this value is within the measurements and theoretical assumptions error to the LFL for downward and spherically propagating premixed hydrogen-air flames of 8.5 - 9.5 vol. %. Thus, any combustion beyond this distance (at smaller concentrations) is "detached" from the area of "continuous" vertical flame [1].

Radial separation distance from hydrogen jet fire requires an analysis of radiative heat transfer rather than flow temperature. Relevant information can be found elsewhere [24].

4.3 Flame lengths and separation distances affected by different issues

4.3.1 The effect of jet attachment on flame length

Table 1. The effect of jet attachment to the ground on its flame length.

Orifice diameter, mm	Flame length, m Attached jets (nozzle 0.11 m above the ground)	Flame length, m Unattached jets (nozzle 1.2 m above the ground)	Flame length increase, times
1.5	5.5	3	× 1.83
3.2	9	6	× 1.50
6.4	11	9	× 1.22
9.5	13	11	× 1.18

It is known from fire safety science that the flame length of fire increases when the fire source is attached to a wall. The effect is even stronger if the same fire is placed in a corner. The phenomenon is explained by the change in the air entrainment rate. Royle and Willoughby [34] measured the increase of the flame length due to the jet attachment to the ground. The flame

length of free unattached horizontal jet from storage at 20.5 MPa through a nozzle located 1.2 m above the ground depends on the nozzle diameter (Table 1).

For attached jet from the nozzle located only 0.11 m above the ground the flame length increases as follows by: 1.83 for nozzle diameter 1.5 mm, 1.50 - nozzle diameter 3.2 mm, 1.22 - nozzle diameter 6.4 mm, and 1.18 nozzle diameter 9.5 mm. The effect of nozzle location above ground on its length growth decreases with the increase of the nozzle diameter.

4.3.2 The effect of nozzle size and shape on flame length

Mogi and Horiguchi [35] studied hydrogen jet flames for spouting pressure 35 MPa and different nozzles diameters, as shown in Figure 17. Five times increase of nozzle diameter from 0.4 mm to 2.0 mm resulted in increase of flame length by five times too - from 1 m to 5 m. This is in line with demonstrated previously dimensionless correlation (6) graphically shown Figure 12: for any given dimensionless ratio L_F/D increase of nozzle diameter D will result in proportional increase of flame length L_F.

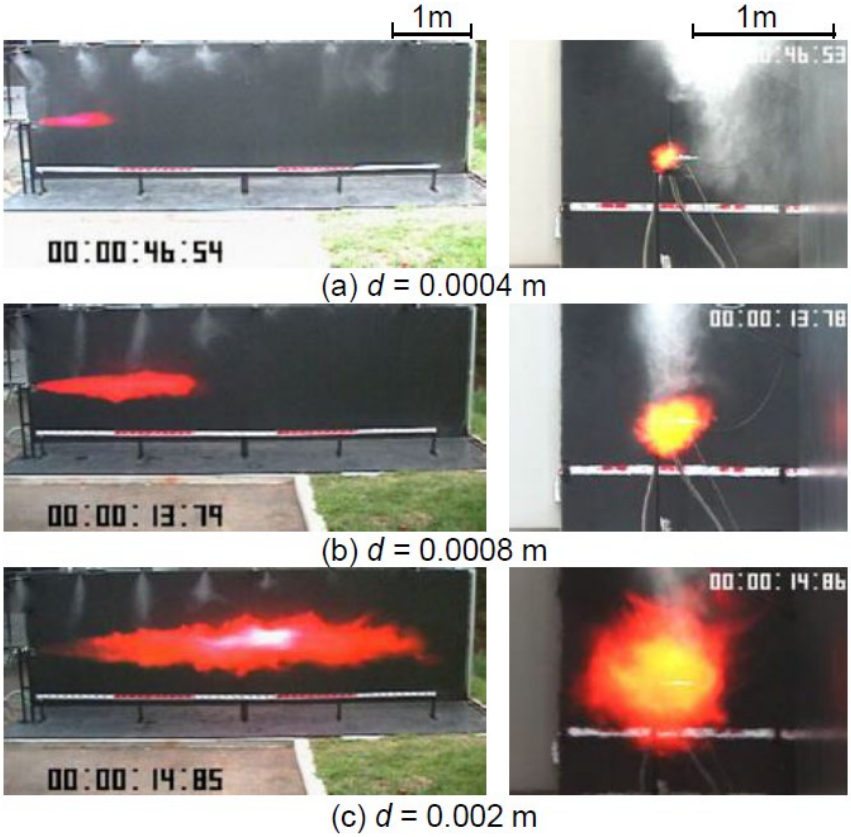

Figure 17. The effect of nozzle diameter on flame length (pressure 35 MPa) [35].

Mogi and Horiguchi [35] also have carried a series of experiments, at release pressure of 40 MPa, studying effect of the nozzle shape on hydrogen flame length and width. Three nozzles of the same cross-section area were tested: the round nozzle 1 mm in diameter, the plane nozzle with size $L \times W = 2 \times 0.4$ mm (aspect ratio (AR) = 5), the plane nozzle of $L \times W = 3.2 \times 0.25$ mm (AR = 12.8). All three nozzles had the same cross section area. Figure 18 shows nozzles images (left), pictures of side view of hydrogen flame from each of three nozzles (center), and

front view of these jet flames (right). The round nozzle flame shape is axisymmetric as in many other experiments. The reacting flow is in the momentum-dominated regime as the effect of buoyancy is not pronounced. However, flames from plane nozzles are flattened in the direction perpendicular to the major axis due to the so called "switch-of-axis" phenomenon, which is the process when the exiting jet expands in the vicinity of the nozzle only in the direction of the minor nozzle axis while it contracts in the major axis direction [36].

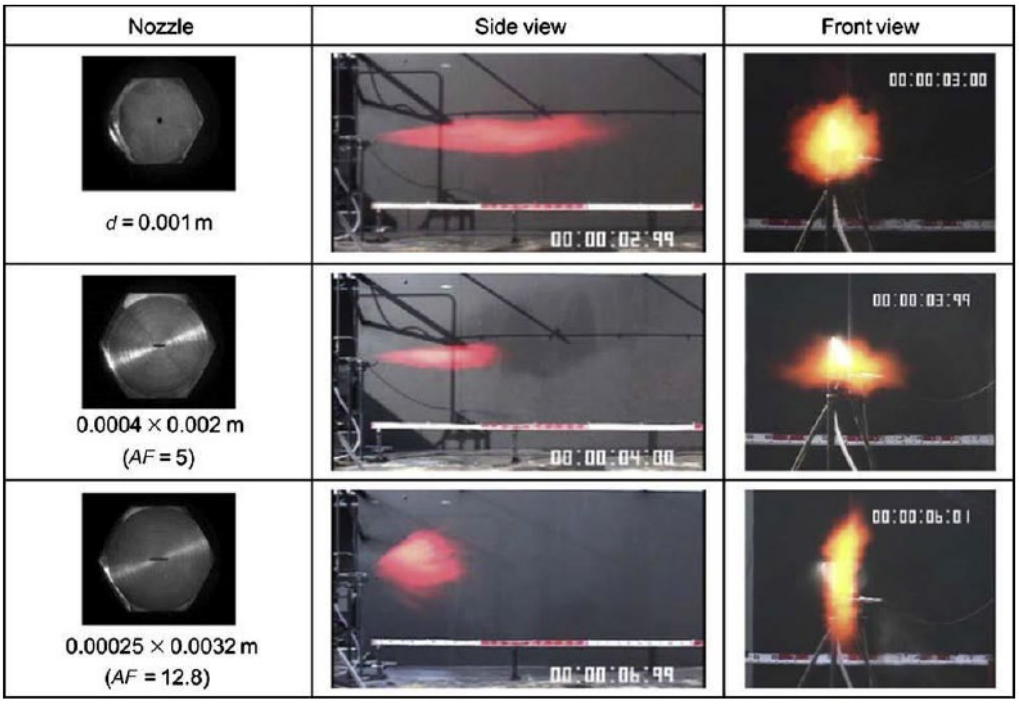

Figure 18. Photographs of three nozzles shape (left), side view of hydrogen flame (centre), and front view of hydrogen flame (right) for release pressure of 40 MPa and different nozzle shapes [35].

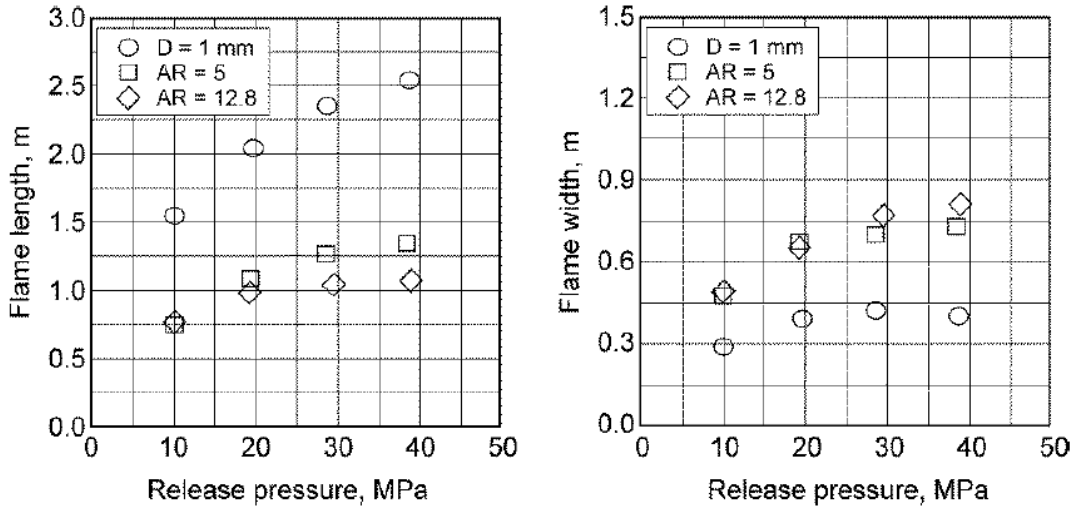

Figure 19. Flame length (left) and flame width (right) for three different nozzles of the same cross-section area: round nozzle of 1 mm diameter, plane nozzle with aspect ratio AR = 5, plane nozzle with AR = 12.8 [35].

The measured flame lengths and widths are presented in Figure 19 [35]. Within tested range of pressures and nozzle sizes the flame length decreased with increase of aspect ratio: for AR = 5 the flame length is approximately twice less compared to the flame from round nozzle, and for AR = 12.8 the flame length is about 2.5 time less. At the same time the maximum flame width for plane nozzles was approximately twice of that for the round nozzle.

4.3.3 The effect of buoyancy on deterministic separation distances

It is also important to know whether a leak is originally momentum- or buoyancy-controlled, or at what axial concentration the flow regime changes from momentum to buoyant part for the same jet. Buoyant jets (lower velocities) are always shorter compared to momentum-dominated jets (high velocities) from the same size nozzle. The simple technique used to distinguish between momentum and buoyancy-controlled flow is based in the work of Shevyakov et al. [38] described in detail in the Lecture 7 - Unignited hydrogen releases outdoors and their mitigation.

4.3.4 The effect of barriers

To reduce the hydrogen flame length, the barriers are often considered as a mitigation measure. However, there is a cost for the reduction of flame length by barriers. For example, in case of vertical 90º barrier the deflagration overpressure peak after delayed ignition (0.8 s) of the turbulent jet from 9.5 mm nozzle at storage pressure 20.5 MPa increases from 16.5 kPa for free jet to 42 kPa [34, 38]. The increase of pressure was recorded at the wall where the release pipe of hydrogen was located and that, on the other hand, the overpressure may be attenuated behind the barrier.



Figure 20. The delayed (0.8 s) ignition of hydrogen jet (20.5 MPa pressure storage, 9.5 mm diameter nozzle) impinging a 90° barrier: deflagration stage (top and middle snapshot), steady-state impinging jet fire stage (bottom snapshot), HSL test [38].

Figure 20 shows a sequence of snapshots (from top to bottom) after the delayed ignition of hydrogen jet impinging a 90° barrier. Before the jet flame reaches the quasi-steady state conditions (bottom snapshot) there is a deflagrative combustion of the non-uniform mixture in the confined space between the barrier and ground (see top and middle snapshots). The inclined to 60° barrier increases overpressure further to 57 kPa. Figure 21 shows two snapshots after the delayed ignition of hydrogen jet impinging a 60° barrier.

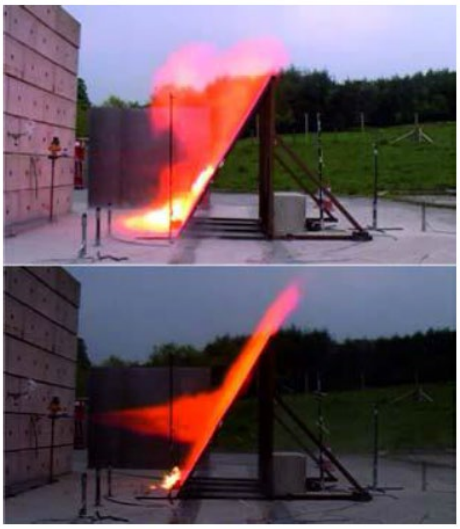

Figure 21. The delayed (0.8 s) ignition of hydrogen jet (20.5 MPa pressure storage, 9.5 mm diameter nozzle) impinging a 60° barrier: deflagration stage (top snapshot), steady-state impinging jet fire stage (bottom snapshot), HSL test [38].

5. Pipeline applications

Gas pipeline is an important artery for domestic and global energy transportation due to the higher safety than transportation by road or rail in terms of incident rates and fatalities. Recent study has demonstrated that the safety performance of natural gas transmission pipelines is superior to that of other transportation modes [60]. A comparative study [61] using incident data collected from 2005 through 2009 in the United States has found the average incident rate for natural gas transmission to be 0.12×10^{-4} per km yr, whereas the incident rate is 0.14×10^{-4} per km yr for road transport of hazardous materials and 1.5×10^{-4} per km yr for railway transport of hazardous materials. In terms of fatalities and serious injuries, gas pipelines are significantly safer.

In addition to natural gas, other gases such as hydrogen and ethylene are transported by high-pressure pipeline. The pipeline transport seems now to be the most cost-effective solution for large-scale distribution of hydrogen as energy carrier, either by adding a larger or smaller fraction of hydrogen in existing natural gas networks or specific networks dedicated to hydrogen. Using the existing pipeline network to convey hydrogen in this way would enable hydrogen production and hydrogen fuelled applications to become established prior to the development of a dedicated hydrogen transportation system, which would require considerable

capital investment and time for construction [62]. The development of a European interconnected Olefins Pipelines network in Europe is planned which will allow this infrastructure to become a true alternative to the other modes of transport (i.e. road, rail). On the other hand, the development of these infrastructures poses the problem of define the hazard area around the pipelines, in order to either set the pipeline at a distance from residential area large enough to avoid any possible damage to people and buildings or to set buildings with a given safety level against potential damage.

During the transportation by pipeline, the main causes of leakage of gas are due to pipelines rupture by the inner or outer factors such as the corrosion, material ageing, and poor quality and so on [63]. Uncontrolled release and ignition of flammable gas may cause a jet fire or an explosion, which are extremely dangerous phenomena for both humans and the surroundings. For a given pipeline, the type of hazard that develops, and the damage or injury potential associated with the hazard, depends on the mode of line failure (i.e., leak vs. rupture), the gas discharge (i.e., vertical vs. inclined jet) and the time to ignition (i.e., immediate vs. delayed). For gases (i.e. CH_4, H_2) with molecular weights significantly less than that of air, the possibility of a significant flash fire resulting from delayed remote ignition is extremely low since a low specific gravity usually precludes the formation of a persistent flammable vapor cloud at ground level. The most common type of fire resulting from the release of gases with high pressure is the jet fire, If the leaked gas with high pressure, jetted out as a jet flow from a crack or a full-bore rupture of the pipeline, is lit at the rupture then the jet fire will happen. In these cases, the effect is strong heat radiation emitted by a long, steady flame with possible damage to the peripheral personnel and buildings [64,65]. Such accidents have been reported as a repeatedly occurring problem due to the complexity of pipeline systems and the human's inability to learn more effectively from those past experiences [66]. The European Industrial Gases Association (EIGA) has provided the frequency data of industrial gas pipeline failures according to the types and magnitudes of pipe leak. Take a 100 mm diameter pipe as an example, the failure frequencies (per metre) for small leak, large leak and break are 6×10^{-6}, 3×10^{-7} and 3×10^{-8}, respectively [67]. A statistic about the jet fire origins (including a total of 84 jet fire accidents from 1961 to 2008) published in the work of Gomez-Mares et al. [68] indicates that pipeline in transport and storage categories represents 11.9% of the total accidents. Once it happens, substantial losses and damages [69] can be imposed to surrounding pipelines, overhead transmission lines and people. Some typical accidents are listed in Table 2.

The hydrogen leakage from high-pressure pipelines could be numerically studied by the same approaches which were used for high-pressure storage tanks. The theories could be found in section 3 of this lecture. Similar to the correlation of the flame length and nozzle diameter (F_L/D) developed by Molkov [1], a new correlation was developed by Wang et al. [70] and their expression showed good agreement with published experimental data as shown in Figure 22.

Table 2 Typical jet fire accidents induced by the leaked high-pressure gas [70].

No.	Date	Location	Pipe diameter (m)	OP/MAP (MPa)	Gas type	Description	Deaths, injuries, and property damage
1	30/07/2004	Ghislenghien, Belgium	1.00	7.00/8.00	Natural gas	The rupture caused tens of vehicles catching fire and liquefying the roof coverings of commercial property within the radius of 150–200 m.	24 deaths, over 120 injuries, and approximately $112 million
2	07/06/2010	Cleburne, Texas, United States	0.91	6.55/7.25	Natural gas	The fire was induced by digging a hole to build a new transmission line. The flame height of more than 250 m was observed.	1 death, 6 injuries, and $1.029 million (for damage and clean-up costs)
3	11/12/2012	Sissonville, West Virginia, United States	0.51	6.41/6.89	Natural gas	The rupture occurred in a sparsely populated area. The total burned area was estimated to be 335 m long by 250 m wide. 3 houses were destroyed and several other houses were damaged.	No fatalities or serious injuries, and $8.685 million (for pipeline repair, system upgrade and gas loss)
4	10/01/2014	Enka, North Carolina, United States	0.30	NA/NA	Natural gas	Overhead transmission lines ignited the leaking gas. The flame more than 30 m high was observed, and the fire lasted about 1.5 h, damaged several cars, houses and commercial buildings.	No one was hurt, and the total loss amounted to $836,720
5	31/07/2014	Kaohsiung, Taiwan, China	0.10	4.25/NA	Propylene	Gas explosions sent flames about 15 stories high in a densely populated area. Over 6 km of roads were destroyed, 3,259 buildings were damaged, and a power grid blackout was initiated, leading to cut power supplies to 12,000 households.	32 deaths, 321 injuries, and an initial loss of $62 million (for rebuilding the damaged roads and drainage system)
6	29/04/2016	Salem Township, Pennsylvania, United States	0.76	7.16/7.24	Natural gas	The fire scorched about 162,000 m^2.	1 injury and unknown property loss

Note: OP, operating pressure; MAP, maximum allowable pressure.

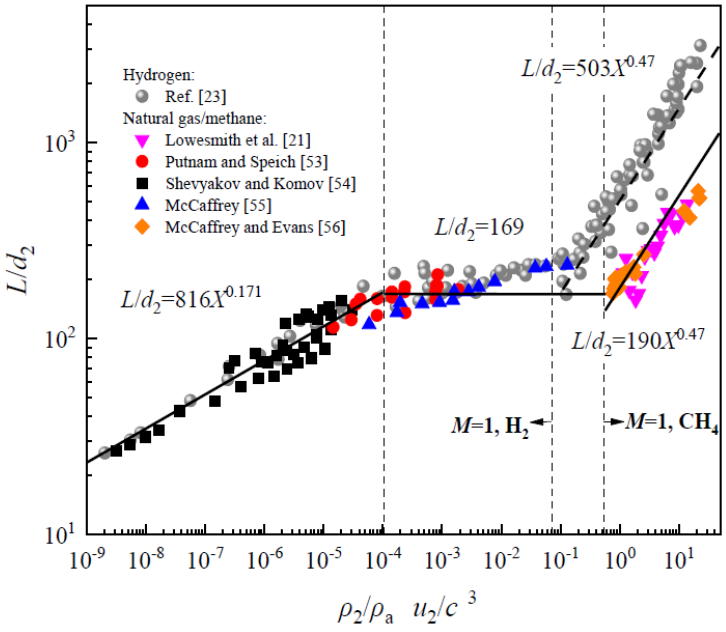

Figure 22. Best-fit equation of Molkov's correlation applied for flame lengths of hydrogen (dashed line) and methane (solid line) jet flames [70]. (L is the flame length and d_2 is the orifice diameter, References in this figure are those in Ref. [70]).

In the work of Coccorullo and Russo [71], a simple and reliable approach for sizing the ground area potentially affected by the failure of high-pressure pipeline was developed. The hazard distance of jet fire, due to the rupture of high-pressure pipeline carrying natural gas, hydrogen and ethylene was evaluated by varying operating pressure, pipeline diameter and length, hole size. Figures 23 shows the effect of pipeline operation parameters on the hazard distance (R) from the pipeline. The results of R for the three gases are reported as function of pipeline diameter (Figure 23a), operating pressure in the case of small leak (Figure 23b) or full-bore rupture of pipeline (Figure 23c) and pipeline length from the gas compression station to the release point (Figure 23d). It can be seen that the hazard distance increases as the pipeline diameter increases because of the increase in the release rate. When increasing the gas pressure inside the pipeline the hazard distance increases. This may be explained as follows: increase of pressure inside the pipeline increases gas density and outlet velocity. Consequently, jet volume and resulting heat radiation increase. Increasing the hole diameter increases the hazard distance, primarily because of the proportional increase in the release rate by comparing Figure 23b and Figure 23c. On the contrary, hazard distance decreases as the pipeline length from the gas compression station to the release point increases. However, the hazard distance remains approximately constant, as the pipeline length gets longer than 3000 m.

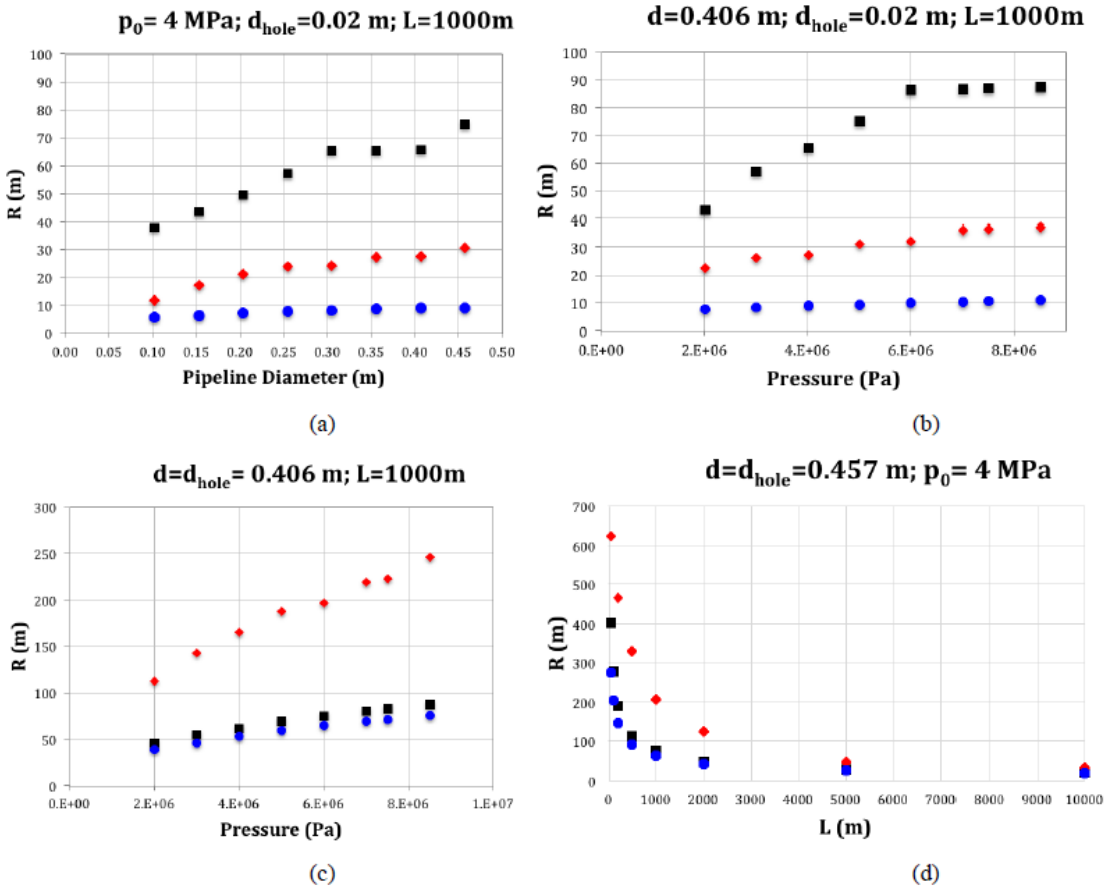

Figure 23. Hazard distance vs (a) pipeline diameter, (b) operating pressure for small leak, (c) operating pressure four full-bore rupture, (d) distance from compression station. black symbol – natural gas, red symbol – ethylene, blue symbol – hydrogen [77].

6. Radiation heat fluxes from jet fires and fireballs

6.1 Radiation heat fluxes from jet fires

Hydrogen burns in a clean atmosphere with an invisible flame. It has a somewhat higher adiabatic premixed flame temperature for a stoichiometric mixture in air of 2,403 K compared to other fuels. This temperature can be a reason for serious injury at an accident scene, especially at clean laboratory environment where the hydrogen flame is practically invisible. However, hydrogen combustion and hot currents will cause changes in the surroundings that can be used to detect the flame. Although the non-luminous hydrogen flame makes visual detection difficult, there is a strong effect of heat and turbulence on the surrounding atmosphere and raising plume of hot combustion products. These changes are called the *signature of the fire.*

The following section is based on the work performed at Ulster in HySAFER centre [7]. Before discussing radiative heat flux, it is worth noting that a hydrogen flame emits minimal infrared radiation and virtually no visible radiation. Due to the absence of CO_2 radiation bands and the strong absorption by ambient water vapour, the ratio of visible to infrared hydrogen jet flames is 0.88 and the ratio of ultraviolet to infrared flame length is 0.78 [39]. Nevertheless, convective and radiative heat fluxes still remain important and must be assessed for the protection of life, property and the environment.

Molina et al. [40] and Schefer et al. [23] developed a model to predict the heat fluxes at any radial (r) and axial (x) position from under-expanded jet fires (see Figure 24) [40].

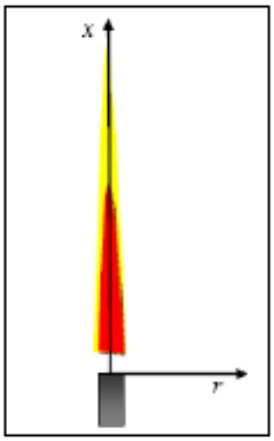

Figure 24. A coordinate system for turbulent jet flame [40].

The use of nominal values nevertheless under-predicts experimental radiative heat flux. To determine radiant heat flux, the following steps have to be followed. It is first necessary to calculate the flame density (air + combustion products) in the flame using the following equation:

$$\rho_f = \frac{P_{amb} M_{sto}}{R T_{ad}} \tag{12}$$

where ρ_f is the flame density in the flame (kg/m^3), P_{amb} is the ambient pressure, M_{sto} is the mean molecular weight of the stoichiometric products of hydrogen combustion in air (24.54 kg/kmol), R is the universal gas constant (8314.47 kJ/kmol·K), and T_{ad} is the adiabatic flame temperature of hydrogen in air. The flame length, width and density are then used in the equation (13) to determine the flame residence time:

$$\tau_F = \frac{\rho_F W_F^2 L_F f_s}{3\rho_{nozz} d_{nozz}^2 U_{nozz}} \tag{13}$$

where τ_F is the residence time (s), W_F is the flame width (assume ratio to length is 0.17), L_F is the flame length, f_s is the mass fraction of fuel at stoichiometric conditions (0.0283), ρ_{nozz} is the density of flow in the nozzle, d_{nozz} is the jet discharge diameter and U_{nozz} is the velocity of flow in the nozzle.

Once the flame residence time is known then it is possible to extract the radiant fraction, X_{rad}, from a figure given by Schefer et al. [23] reproduced in Figure 25, where X_{rad} is the fraction of total chemical heat release that is radiated to the surroundings. It should be noted that for a small flame, the approach suggested by Schefer et al. [23] could not be used because L is small and then the radiant fraction is negative.

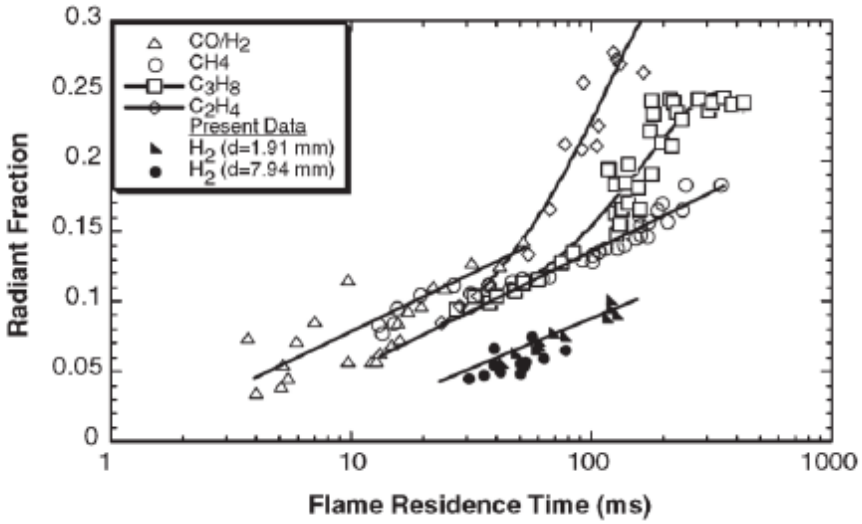

Figure 25. Radiant fraction as a function of flame residence time [23].

The radiant fraction is then implemented in the equation (14) to extract S_{rad}, the total emitted radiative power:

$$S_{rad} = X_{rad} \dot{m}_{nozz} \Delta H_c \tag{14}$$

where S_{rad} is the total emitted radiative power (W), $\dot{m}_{nozz}$ is the mass flow rate at the nozzle and ΔHc is the heat of combustion of hydrogen. The coordinates x and r can be chosen in two ways:

- Option 1: The coordinates can be chosen. In that case they can correspond to the location of possible targets of a jet fire: occupants, building, escape routes, other source of

potential hazards like storage of flammable or toxic substance, etc. When coordinates are chosen, the first step is to calculate L_F. Then, it is easy to calculate the non-dimensional radiant power C^* using the desired value of x (m), the position on the jet axis from the nozzle. This can be done using the Figure 26. Finally, by setting the r value, $q_{rad}\ (x,r)$ is calculated with the equation (15).

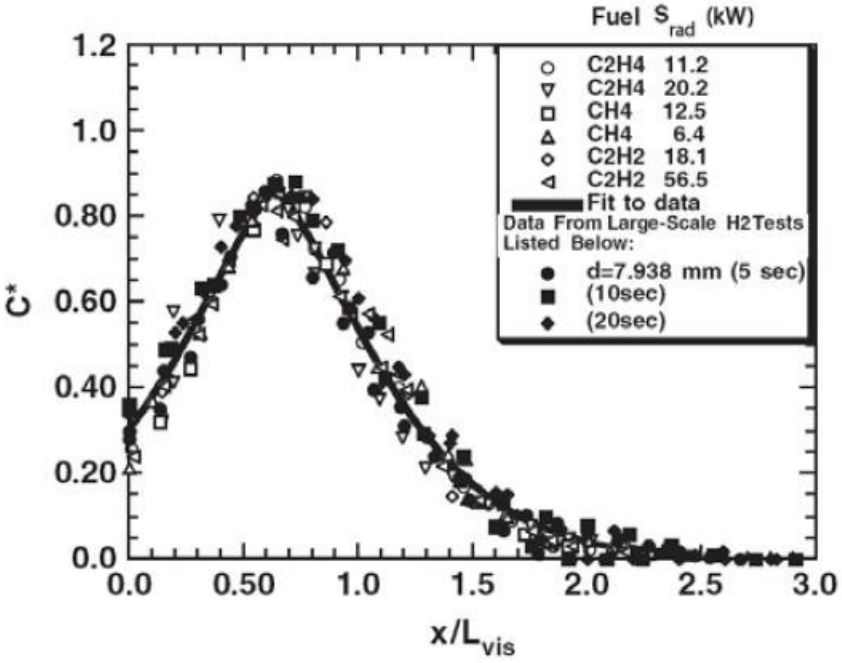

Figure 26. Axial variation of normalized radiative heat flux [23].

- Option 2: The coordinates can be calculated for a chosen value of radiative heat flux. It means that the calculated coordinates form contour around the jet fire corresponding to a particular iso-value of radiative heat flux. The value of the radiative heat flux can be defined e.g. as acceptance criteria. The flame length, flame width, residence time, radiant fraction and the total emitted radiative power have to be calculated. Then, the value of the non-dimensional radiant power can be calculated using appropriate equation for each value of x in the desired range. Finally, r can be calculated for each axial position by implementing in the equation (15) the corresponding value of C^* and the chosen radiant heat flux:

$$q_{rad}(x,y) = \frac{C^* S_{rad}}{4\pi r^2} \tag{15}$$

where $q_{rad}\ (x, r)$ is the radiative heat flux at the location (x, r) (W/m^2), C^* is the non-dimensional radiant power from Figure 26, and r is the radial position from the jet centerline (m).

It should be noted that the above analysis is based on a vertical flame. It is not clear yet what the effects will be when a flame is horizontal. Buoyancy may influence the flame and thus at this stage it is hard to estimate how the downstream hot currents will behave. Thus, the

approach described above may be somewhat conservative in the case of a horizontal flame. Effect of radiative heat flux on people, environment and structures is discussed in detail in the Lecture 6 - Harm criteria for people and property.

6.2 Hydrogen jet fires versus jet fires of common fuels

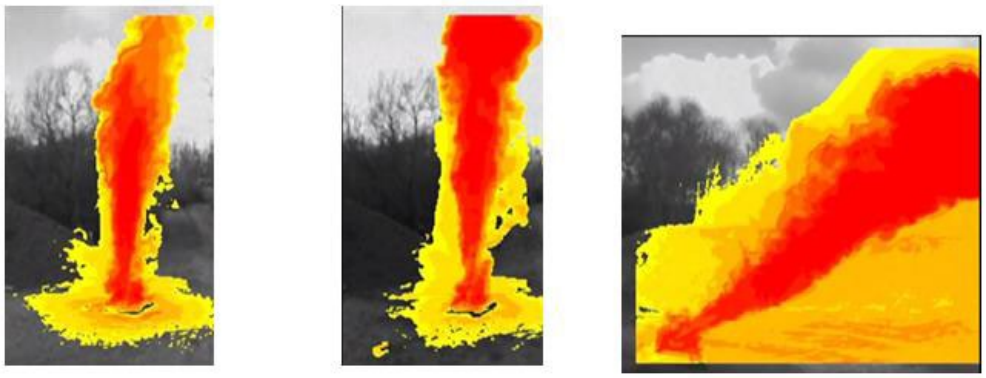

Figure 27. Infrared image of jet fires showing thermal radiation produced by combustion of hydrogen (200 bar), CNG (200 bar) and LPG (10 bar).

As it follows from Figure 27, due to the incomplete combustion, CNG and LPG produce CO_2, CO, soot, and other products, which have higher effect on the radiation compared to hydrogen. This phenomenon explains why hydrogen combustion is characterised by lower thermal effects than other common fuels, even if the temperature exceeds the one of a CNG flame. Figure 27 shows comparison of thermal radiation produced by hydrogen (200 bar), CNG (200 bar) and LPG (10 bar) – thermal signature of hydrogen jet fire is slightly smaller than that of CNG, and both of them are significantly smaller than thermal radiation from LPG fire.

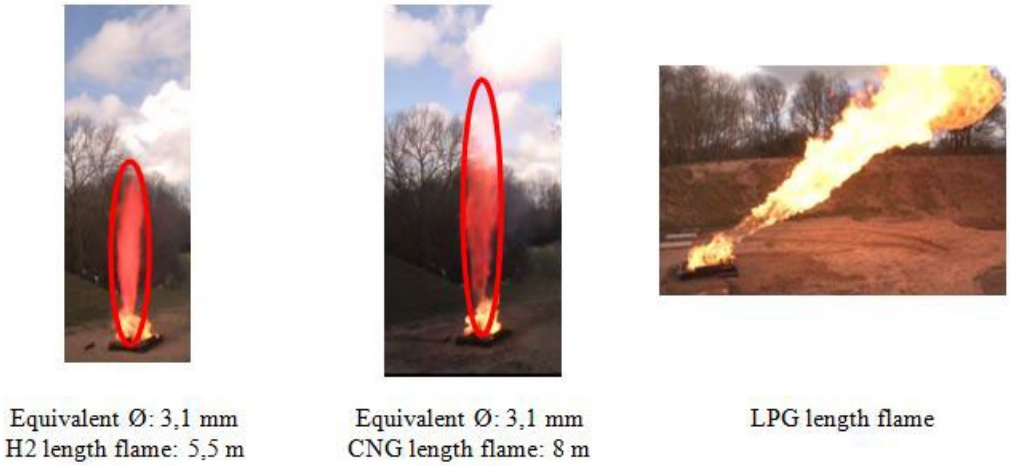

Figure 28. Comparison of the flame lengths for jet fires of hydrogen (orifice diameter 3.1 mm), CNG (orifice diameter 3.1 mm), and LPG.

As it is shown in Figure 28, for the same flow rate, due to the oxygen consumption, which is 4 times higher for CNG and 5 times higher for LPG than for hydrogen, the flame lengths of CNG and LPG jet fires are longer than the hydrogen flame length.

It is important to remember that hydrogen flame is not visible in a pure environment. However, for FCH systems and infrastructure applications there are always combustible materials present, which will colour the flame as it shown in Figure 28.

6.3 Hydrogen fireballs

Hydrogen fireballs can be produced as a result of a hydrogen storage tank catastrophic failure. The case for safety published on "h2safe.net" resource (http://h2safe.net/case_safety.html) [41] analyses relative frequencies of failure modes and states that only about 10 - 27% of pressurised gas releases are classified as catastrophic. Nevertheless, it must be stressed that the malfunction of the tank safety device, TPRD, can lead to a catastrophic rupture of the hydrogen storage tank. UU has worked on modelling the catastrophic rupture consequences and effects, focusing on heat radiation and blast waves. The sizes of fireball reported by Zalosh [42] can be used as a guidance. The experiments related to a catastrophic failure of hydrogen storage tank were carried out on a stand-alone vessel (type IV tank; volume 72.4 L; storage pressure 34.3 MPa; no TPRD) and the vessel installed underneath a sport utility vehicle (type III tank, volume 88 L; storage pressure 31.8 MPa, no TPRD). Type IV stand-alone tank catastrophically failed after 6 min 27 s from the start of the fire. It was followed by a fireball of 7.7 m in diameter, 45 ms after tank rupture. This fireball was lifted in 1 s [42].

For the type III tank under vehicle, after approximately 4 minutes of exposure to the propane bonfire, flames and gases entered the passenger compartment. The catastrophic tank rupture occurred after 12 minutes 8 seconds of fire exposition, generating a fireball with maximum diameter of 24 m and lasting 4.5 seconds. Various parts of the test vehicle and storage tank were found at distances up to 107 m. It must be stressed that the above-mentioned distances can be even longer for the hydrogen storage tanks pressurized to 70 MPa [42].

The development and validation of the CFD model to simulate blast wave and fireball dynamics after stand-alone high-pressure hydrogen tank rupture in a fire in the open atmosphere were recently done by Molkov et al. in UU [72]. The complementarities and synergy of experimental data and numerical analysis allowed to get insights into blast wave and fireball dynamics, and thus close knowledge gaps in understanding of underlying physical phenomena. This was the first study quantitatively explaining the mechanism of hydrogen combustion contribution to the blast wave strength. For example, hydrogen combustion after 36 L 70 MPa tank rupture in a fire increases the maximum blast wave overpressure at 5 m by 37%. The simulated fireball was seen to display typical development during a growth stage before rising with buoyancy effects. The fireball size and shape (7.7 m after 45 ms) was accurately reproduced in the USA experiment.

6.4 Effect of delayed ignition on the pressure of hydrogen jet fires

There is an unsteady stage in the jet establishment immediately after leak initiation from the high-pressure hydrogen equipment. Delayed ignition and consequent combustion of the unsteady highly turbulent hydrogen-air cloud formed at this stage can lead to significant

overpressure in the near field able to harm people. This process is basically the deflagration and takes place before the quasi-steady jet fire is established [1].

The UK Health and Safety Laboratory (HSL) of the Health and Safety Executive performed a series of over 40 experiments with high-pressure releases of hydrogen as a part of the project HYPER [38] and published later by Royle and Willoughby [34]. The effects on overpressure of the varying jet exit diameter, the ignition delay and position were determined.

Hydrogen was stored in two 50 liters cylinders at pressure 20.5 MPa. There was a stainless-steel tubing of internal diameter 11.9 mm, and a series of ball valves with internal bore diameter of 9.5 mm between the storage and the nozzle exit. Restrictors of the same 2 mm length and different diameter of 1.5, 3.2, and 6.4 mm were used in the nozzle to vary the jet exit diameter. The release point was 1.2 m above the ground. The jet was ignited by a match head with small amount of pyrotechnic material 1.2 m above the ground. The ignition point location varied in the range 2 - 10 m from the release point. Piezo-resistive transducers were pointed out upwards except for wall mounted. Three transducers were located at perpendicular to the axis distance 1.5 m, 2.6 and 3.7 m, at height 0.5 m [34]; axial distance of all transducers was 2.8 m from the nozzle and height was 0.5 m.

Time 260 ms was needed to fully open the valve, 140 ms for hydrogen to reach 2 m. Thus, 400 ms is the shortest possible ignition delay of the unsteady jet. Jets from hydrogen storage at 20.5 MPa were predominantly momentum-controlled, i.e. the flow was relatively non-buoyant up to the lower flammability limit [34].

6.5 Effect of various parameters on overpressure

6.5.1 The effect of an orifice diameter on overpressure

Table 3 shows experimental measurements of the unsteady hydrogen jet deflagration overpressure for two ignition delays (minimum possible 400 ms and 800 ms) and nozzle diameters from minimum 1.5 mm to maximum 9.5 mm. The nozzle diameter has a crucial effect on the maximum overpressure generated by ignited jet.

There was no recordable overpressure for release through the nozzle of 1.5 mm diameter. The overpressure for 400 ms ignition delay, when jet just reached the ignition point located 2 m downstream from the nozzle, is always below the overpressure for the ignition delay of 800 ms corresponding to a larger turbulent flammable hydrogen-air cloud formed. It is worth noting that there is a wall in the experiments behind the nozzle. The maximum registered overpressure of free hydrogen jet was 16.5 kPa.

There is an important conclusion from this series of experiments: the leak diameter has to be reduced as low as reasonably possible (ALARP) for a particular FCH technology. The inclusion of flow restrictors in hydrogen supply lines reduces the flame lengths observed, therefore reducing safety distances required. This is thought due to reduction of mass flow rate and pressure losses on the restrictor and thus lower pressure at the jet exit from the pipe.

Table 3. The effect of an orifice diameter and the ignition delay on the maximum overpressure generated by deflagrating jet [34].

Orifice diameter, mm	Ignition delay, ms	Max overpressure, kPa
1.5	800	Not recordable
1.5	400	Not recordable
3.2	800	3.5
3.2	400	2.1
6.4	800	15.2
6.4	400	2.7-3.7
9.5	800	16.5
9.5	400	3.3-5.4

It was concluded that the jet turbulence and the size had a greater effect on a deflagration pressure than the total amount of hydrogen leaked. The total amount of hydrogen released is not always important, especially at open atmosphere, as buoyancy continues to drive dilution of hydrogen by entrained air until it reaches the LFL of 4 vol. % and beyond. Thus, portions of hydrogen released in the beginning in many practical scenarios will not contribute to the combustion as they form a part of cloud which is below the LFL [34].

It can be assumed, based on the presented results, that the spontaneous ignition of a sudden hydrogen release by the diffusion mechanism could reduce overpressure of self-ignited release compared to the delayed ignition (the ignition delay is minimised in this case). It is worth noting that the spontaneous ignition was observed during sudden release in case of rupture disk burst and the scenarios of spontaneous ignition of jet by the diffusion mechanism, when valves were used to initiate the high pressure hydrogen release, is not included [1].

6.5.2 The effect of the ignition delay on overpressure

The effect of the ignition delay was studied for the nozzle diameter 6.4 mm and the ignition location of 2 m from the nozzle (as demonstrated in Table 4). It can be concluded that ignition in a close to the flammability limits region of the jet cloud (ignition delay of 400 ms) results in a relatively slow burn and hence a small overpressure. The maximum overpressure of 19.4 kPa is observed for the ignition delay of 600 ms. Maximum overpressures were observed when the jet was ignited at a time which coincided with the area of maximum turbulence within the front portion of the jet, reaching the ignition point.

Table 4. The effect of ignition delay on the maximum overpressure generated by deflagrating jet [34].

Ignition delay, ms	Max overpressure, kPa
400	3.7
500	18.4
600	19.4
800	15.2
1000	11.7
1200	12.5
2000	9.5

6.5.3 The effect of ignition source location on overpressure

A single nozzle with diameter 6.4 mm was chosen with a fixed release pressure of 20.5 MPa and a fixed ignition delay 800 ms. The ignition position varied from 2 m to 10 m. The maximum overpressures were seen by transducer No.1 located 2.8 m from the nozzle and 1.5 from the jet center line (Table 5). The deflagration overpressure reduces drastically with the increase of the ignition position from the jet source. There was no ignition of jet with the location of the ignition source 10 m from the nozzle.

Table 5. The effect of the ignition source position on the maximum overpressure generated by deflagrating jet [34].

Ignition position, m	Max overpressure, kPa
3	5.0
4	2.1
5	2.1
6	Not recordable
8	Not recordable
10	No ignition

7. Fire of FC vehicles

Fuel Cell Vehicles (FCVs) are one of the main fast developing applications of FCH technologies. Similar to a battery-electric car, a fuel cell car does not have the internal combustion engine. Fuel cells convert the energy stored in chemical form directly into electrical energy that powers the cars. Worldwide, several thousand FCV have been established, and small fleets of fuel cell cars are being used especially by companies and government agencies but also private persons. These include released serial models from Hyundai (iX35 fuel cell and NEXO) and Toyota Mirai I and II modelsMore than a thousand cars running in Germany with a hundred refilling stations in operation! Also, some fire brigade cars are already fuel cell vehicles.

As an example, according to fire statistics in Great Britain [43], in the UK, 28,800 road vehicle fires were registered in 2011-2012. For comparison, in USA 172,500 automobile fires occurred

in the same period. Different types of vehicles were affected: motor cars, heavy goods vehicles, light goods vehicles, public transport vehicles etc. The majority (65 %) of fires occurred in cars, 10 % were in vans, 4 % were in lorries and 2 % in buses or minibuses [43]. Fire causes can be accidental, deliberate, or unknown. The majority of deliberate fires (43%) involved road vehicles: 13,900 fires. The number of fatalities in road vehicle fires in 2011-12 was 37 [43].

During period from 2000 to 2006, 20 catastrophic CNG tank failures were documented, 11 of them have been attributed to vehicle fires [44]. Of these 11 incidents, the evidence suggests that the majority of the PRDs failed to activate (in case of a localized fire). “Testing has shown that all fuel tanks (both CNG and hydrogen) regardless of working pressure are highly susceptible to rapid degradation due to localized fires” [44]. This means that catastrophic failure cannot be ruled out of the risk assessment [41].

Hazards and associated risks for FCVs should be proven and interpreted in a professional way, with the full comprehension of consequences by all stakeholders, starting from FC system designers through regulators to users. The first comparison of the “severity” of a hydrogen and gasoline (petrol) fuel leaks and ignitions was performed by Swain [45]. Figure 29 shows the snapshots of hydrogen jet fire and gasoline fire at 3 s (left) and 60 s (right) after a car fire initiation. It should be noted that these early images do NOT reflect more recent angled and smaller diameter TPRD design.



Figure 29. Hydrogen jet fire and gasoline fire: 3 s (left) and 60 s (right) after a car fire initiation [45].

The scenario with a hydrogen-powered car presented in Figure 29 is rare. (Please note in FCV vehicles the release of hydrogen will not be oriented vertically upward.) It can be realised at a false self-initiation of a pressure relief device (PRD). Indeed, a release of hydrogen through the PRD from the on-board storage would be in majority of cases initiated by an external fire. A scenario with the external fire drastically changes hazards and associated risks compared to the situation shown in Figure 29.



Figure 30. A FCV gasoline pool fire test: left – gasoline fire just before initiation of TPRD, right – 1 second after TPRD initiation [46].

Figures 30 and 31 demonstrate the results of a study on hydrogen-powered cars fire performed in Japan [46]. The FCV was equipped with a thermal pressure relief device (TPRD) with a vent pipe internal diameter of 4.2 mm. In a test shown in Figure 30 the compressed hydrogen tank was installed exactly at the position of the removed gasoline tank. By this reason, there was no chance to install a larger storage vessel and a small tank of 36 L at pressure 70 MPa was used. The fire spread from a gasoline vehicle to FCV was investigated to address scenarios when different types of vehicles are catching fire in car collision or natural disaster like earthquake. The experiment revealed that when the TPRD of FCV's storage tank is activated by gasoline fire a fireball of more than 10 m diameter is formed (Figure 30, right).

In another test of Tamura et al. [46], two vehicles were parked approximately 0.85 m apart and the spread of fire from FCV to the gasoline vehicle was investigated. Figure 31 shows two vehicles after the TPRD initiation in the FCV. It can be concluded that self-evacuation from the car or safeguarding by First Responders with such design of hydrogen release system is impossible and car manufacturers yet must address this customer safety issue.



Figure 31. The HFCV with initiated TPRD (on the left) and the gasoline car (on the right) [46].

In the test conditions the cause of fire spread from the FCV to the adjacent gasoline vehicle is the flame spreading from the interior and exterior fittings of the FCV, but not the hydrogen flame from the TPRD (it is worth noting that the small storage tank of only 36 litres with a shorter hydrogen release time was used in the study by Tamura et al. [46] instead of a larger tank that is needed to provide competitive driving range). The authors concluded that in car carrier ships and other similar situations with closely parked FCVs, the test results point to the possibilities of a fire in an FCV to activate its TPRD and thereby to generate hydrogen flames which in turn may cause the under floor TPRD activation in adjoining FCV.

To minimize the damage by FCV fire authors of [46] suggested that it is important to early detect and extinguish fire before the TPRD activation. It is known that hydrogen fire is difficult if not possible to extinguish in many practical situations. Hopefully, car manufacturers will develop appropriate safety engineering solutions, including reduction of flame length from hydrogen-powered vehicle in a mishap, thus excluding the possible "domino" effect in accident development and assisting first responders to control such fires and successfully perform rescue operations. The experiments carried out by Tamura et al. have clearly demonstrated that FCV's fire consequences can be very "challenging" both from life, safety and property loss points of view [46].

As it was mentioned earlier, compressed gaseous hydrogen is currently the mainstream technology for on-board hydrogen storage. The pressure for on-board storage is up to 70 MPa. Type IV tanks (with polymeric liner) are normally used. Unfortunately, the fire resistance of these tanks is low. For example, Stephenson [47] have reported the time to catastrophic failure in the range from 3.5 to 6.5 minutes. Current "solution" to prevent the catastrophic of failure of these tanks in fire conditions is to release hydrogen quickly, through a TPRD with an orifice of a comparatively large diameter (up to about 5 mm) before the failure. However, this "solution" is unacceptable, even in the open atmosphere, due to the long flames, preventing safe evacuation and rescue operations (Figure 32). Additionally, it creates a serious problem for life safety and property protection when FCV is located in a confined space like garages, tunnels or car parks [21].



Figure 32. Hydrogen jet flame from a PRD of an FCV oriented upwards [48]. (NOTE current TPRDs tend to be angled)

The fire, shown in Figure 32, was initiated on the ashtray of the instrumentation panel [48]. The PRD was directed upwards and activated 14 min 36 s after the fire initiation (upward scenario). Tested FCV was equipped with two 34 L capacity cylinders at 35 MPa each and PRD diameter of 5 mm (to allow blow-down on hydrogen in 5 min before the catastrophic rupture).

The scenario with a downward hydrogen release from a PRD is represented in Figure 33. The PRD was activated, in this case, at 16 min 16 s after fire initiation [48].



Figure 33. Hydrogen jet flame from a PRD of an FCV oriented downwards (left – car back view; right – car side view) [48].

Figures 32 and 33 demonstrate that current design of TPRD in case of hydrogen release and jet fire does not allow self-evacuation of car driver and passengers, prohibits intervention of responders and create hazards for public. The release of hydrogen from a TPRD can be considered as a typical accident scenario. When the temperature reaches more than 110 °C, the TPRD activates and hydrogen is released. TPRDs are commonly located on storage tanks, underneath of FCVs. The release is orientated vertically downwards, and the hydrogen flame will impinge on the ground. An ignited release from a TPRD is most likely to occur in an event of a car fire, independent of whether the car is parked or driven on a road. The hazards associated with this scenario depend on the ignition time. In the case of immediate ignition, the impinging hydrogen jet flame (under the car) will spread outwards and create a high temperature fire environment, which is hazardous to people and property. Without immediate ignition, the released hydrogen will form a flammable cloud that has a potential to result in a delayed ignition.

In the studies at Ulster University, the deterministic separation distances for ignited releases in the open atmosphere are evaluated [49]. For ignited releases, three temperature limits were adopted as harm criteria for different vulnerable targets. For the general public, a temperature of 70 °C was taken as an acceptance criterion for no harm. For the responders without thermal protective clothing, a temperature of 115 °C was assumed to be the pain limit. For responders with thermal protective clothing, it was conservatively assumed that they should not work in

an environment where the temperature is higher than 260 °C, as the bunker gear is designed not to ignite, melt, drip, or separate when exposed to such temperatures for five minutes [50].

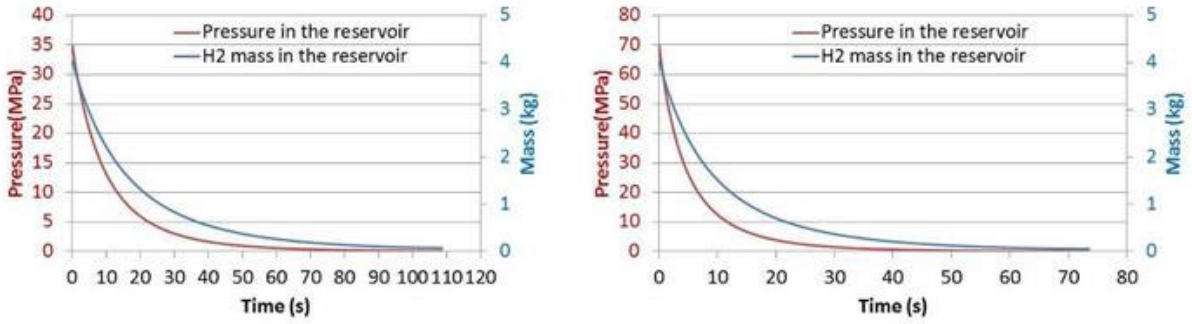

Figure 34. Pressure and mass dynamics in a hydrogen storage tank during blow-down through 4.2 mm TPRD orifice: 171 L tank, initial pressure 35 MPa (left), and 101 L tank, initial pressure 70 MPa (right) [49].

In real-world conditions, a hydrogen release from a high-pressure tank is not a steady-state one but a blow-down process, with pressure decaying in the reservoir until the tank is empty. The notional nozzle model mentioned above can be applied to simulate pressure dynamics in the hydrogen storage tank during an under-expanded jet release. Figure 34 shows pressure and mass dynamics during blowdown from two hydrogen storage tanks: 171 L volume, 35 MPa storage pressure (Figure 34 left), and 101 L, 70 MPa storage pressure (Figure 34 right). Both tanks contain initially the same amount of hydrogen of 4.05 kg, and have the same TPRD orifice diameter of 4.2 mm. As it follows from Figure 34 the total blow-down time even for 35 MPa storage pressure is less than 110 s, and the transition from an under-expanded jet to an expanded one occurs at 85 s. For the release from 70 MPa storage tank the total blow-down time is less than 75 s, with the transition from an under-expanded jet to an expanded jet occurring at about 58 s [49].

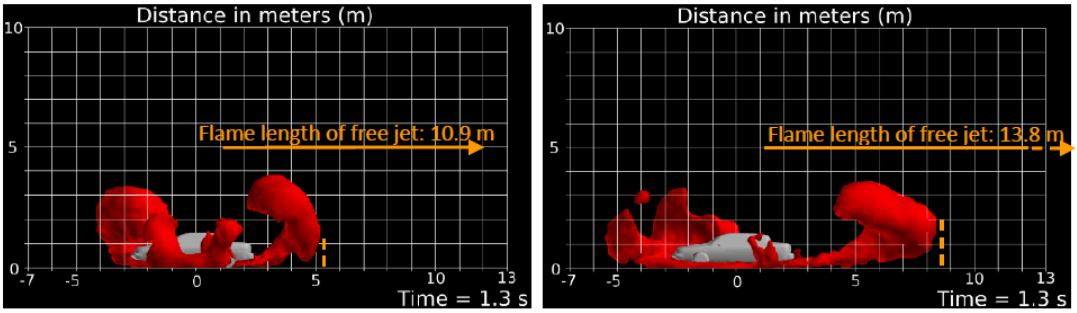

35 MPa 70 MPa

Figure 35. Side view of the largest hydrogen flame envelope (iso-surface of temperature T = 1,300 °C) [49].

Figure 35 shows a snapshot of the largest flame envelope resulting from hydrogen release via a 4.2 mm orifice TPRD installed under a car and directed downwards. The flame envelope was obtained in CFD simulations and visualised using temperature iso-surface T = 1,300 °C. The

longest flame tip location is about 5.2 m and 8.4 m for releases from storage with pressures 35 MPa and 70 MPa respectively. The flame length for the 70 MPa release increases more than 60% compared with that of the 35 MPa release. For both cases, the largest flame envelopes near the ground occur at about 1.3 s after the opening of the TPRD. Afterwards, the flame will shrink, and the separation distances will decrease. Figure 35 also shows the longest flame propagation for unobstructed free jet fires calculated using analytical correlation (6) (also shown in Figure 12). Realistic release from under-car TPRD results in a significant reduction of the flame envelope - more than 50% and nearly 40% for releases from storage with pressure 35 MPa and 70 MPa respectively [49].

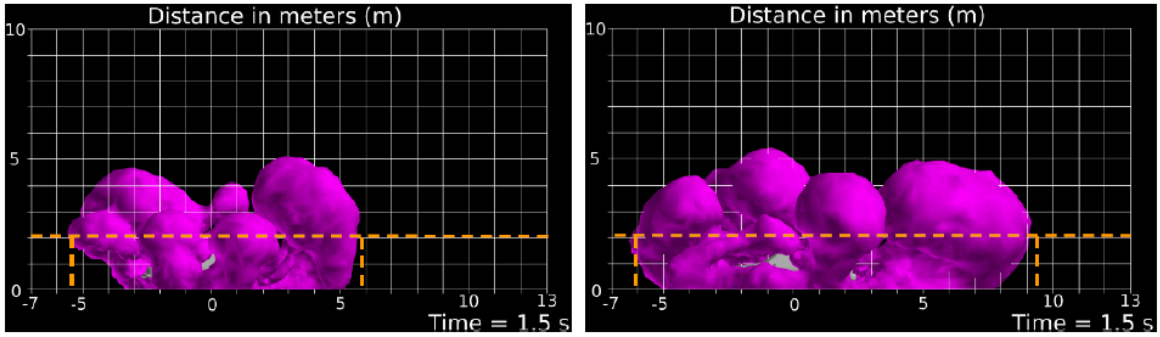

35 MPa 70 MPa

Figure 36. Side view of the largest envelop for safe operation of responders in protecting clothing (iso-surface of temperature $T = 260$ °C) cut off at 2 m height [49].

Figure 36 shows temperature iso-surface $T = 260$ °C corresponding to the safety threshold for operation of responders in thermal protective clothes. The longest hazard distance is about 5.8 m and 9.2 m for releases from storage with pressures 35 MPa and 70 MPa respectively. The hazard distance for the 70 MPa release increases more than 58% compared to that of 35 MPa release. For both cases, the largest 260 °C temperature envelopes near the ground occur at about 1.5 s after the opening of the TPRD. Afterwards the envelopes will shrink, and the separation distances will decrease [49].

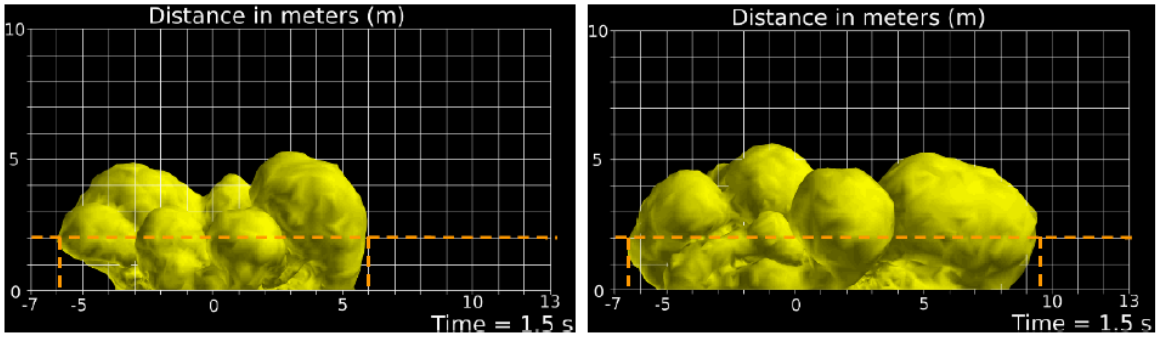

35 MPa 70 MPa

Figure 37. Side view of the largest envelop for safe operation of responders without protecting clothing (iso-surface of temperature $T = 115$ °C) cut-off at 2 m height [49].

Temperature T = 115 °C iso-surface corresponding to threshold for operation of responders without protective clothing is shown in Figure 37. The longest hazard distance in this case is about 6 m and 9.4 m for releases from 35 MPa and 70 MPa storage pressure tanks, respectively. The hazard distance for the 70 MPa release increases nearly 57% compared to that of the 35 MPa release. For both cases, the largest envelopes corresponding to the temperature T = 115 °C and near the ground occur at about 1.5 s after the opening of the TPRD. Afterwards, the envelopes will shrink, and the separation distances will decrease [49].

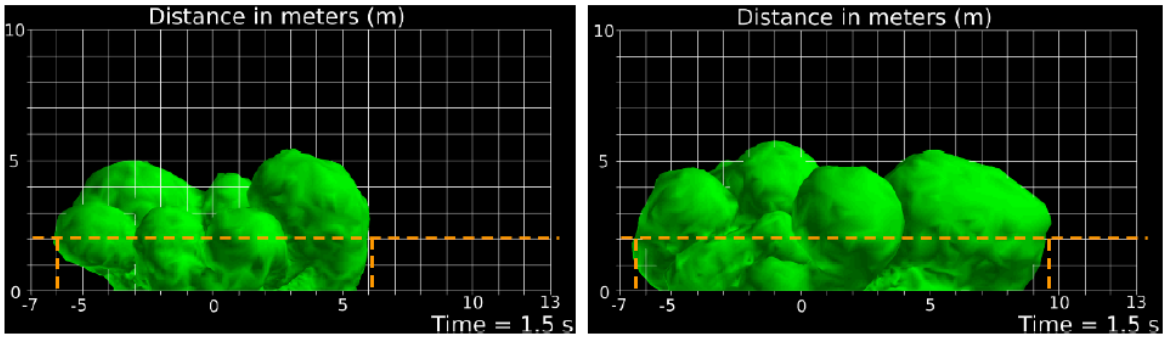

35 MPa 70 MPa

Figure 38. Side view of the largest envelop for public safety (iso-surface of temperature T = 70 °C), cut-off at 2 m height [49].

It can be seen from Figure 38 that for the general public, the longest separation distance is about 6 m and 9.5 m, for the 35 MPa and 70 MPa releases, respectively. The separation distance for the 70 MPa release increases more than 58% compared with that of the 35 MPa release. For both cases, the largest 70 °C temperature envelopes near the ground occur at about 1.5 seconds after the opening of the TPRD. Afterwards, the envelopes will shrink, and the hazard distances will decrease [49].

In addition, the sound levels associated with hydrogen leaking and explosion also need consideration.

8. Detection, mitigation and extinction of hydrogen fires

8.1 Detection of hydrogen fires

The fire detection system is typically configured to provide an audible/visual alarm and/or activate a fire suppression system. There are various approaches to detecting a fire, based on:

- Heat detection,
- Frangible bulbs,
- Fusible plugs,
- Rate compensated heat detectors,
- Linear heat detection (cables routed through fire risk areas),

- Ionisation smoke detection,
- Optical smoke (obscuration/line-of-sight) detection,
- Gaseous products of combustion detection, e.g. CO, volatile organic compounds,
- Optical flame detection (IR and UV and combined IR-UV),
- High-speed and high sensitivity smoke detection,
- Closed-circuit television (CCTV) based systems [21].

As stated earlier hydrogen burns with a pale-blue flame (in clean environments) and emits neither visible light in day time (sun radiation can overpower the hydrogen flame light) nor smoke unless e.g. sodium is added or dust particles are entrained and burned along with the combustible mixture. Compared to hydrocarbon combustion, hydrogen flames radiate significantly less heat and so human physical perception of this heat does not occur until direct contact is made with the flame. Therefore, hydrogen fire may remain undetected and propagate in spite of any human direct monitoring in the areas where hydrogen can leak, spill or accumulate, forming potentially combustible mixtures. Hydrogen fire detectors can help to take immediate actions in these situations. Hydrogen fire detectors can be either fixed for continuous monitoring of remote operations or portable for field operations.

Some most common types of hydrogen detectors are summarised in Table 6 and described in detail in the following sections.

Table 6. Types of fire detectors suitable for hydrogen flames.

Type	Advantages	Drawbacks
UV/IR	Moderate speed Moderate sensitivity Low false alarm rate Not blinded by CO_2 fire protections discharges Automatic self-test	False alarms possible in case of combination of IR and UV sources Blinded by thick smoke and vapours Price
Triple IR	Very high sensitivity Very high speed	Price
IR/vis imaging	Images the flame Used by NASA	Price

For an efficient and a reliable use, a hydrogen fire detector should fulfil the following criteria:

- pick up every true alarm;
- avoid false alarms;
- be specific and pick up hydrogen fire signals among various ones that become even more numerous when detector sensitivity is increased;

- a limited response time especially if it triggers a safety action.

Hydrogen fires tend to emit radiation over a broad range of wavelengths and are not characterised by extreme peaks for particular frequencies. Hydrogen fire detectors can also rely on UV and IR light detection. Besides the radiation itself, hydrogen flames can be indirectly visible by their strong heat effect and turbulence, so called “heat ripples” of the surrounding atmosphere. Optical flame detectors detect specific spectral radiation emitted during the combustion process by the various chemical species (ions, radicals, molecules) that are either intermediates or final products of combustion. Chemical species emit radiation at wavelengths characteristic to the particular species.

The hydroxyl radical (OH) and water (H_2O) are the main emitting chemical species in the hydrogen combustion process. These species emit radiation at specific spectral bands, according to their electronic structure and the typical energy (translation, vibration, rotation) of the process.

- OH (being an active intermediate radical with an available free electron) emits strongly in the UV spectral band at the 0.306 and 0.282 µm peak and additional weaker emission peaks at 0.180 - 0.240 µm. It also emits infrared energy in the near IR band (vibration and rotation of the molecule) with several peaks within the 1-3 µm spectral band.
- H_2O emits mainly in the near IR band (vibration and rotation) with strong peaks at 2.7; 1.9 and 1.4 µm, ranging from the highest to the lowest intensity.

These detection techniques assume that no interfering shield is placed between the flame and the UV/IR detector. Though optical techniques are available to pick up these various wavelengths, the main challenge consists in discriminating hydrogen flame emitted signals with other potential sources that emit similar signals in frequency and intensity.

8.1.1 UV detectors

UV systems are favoured to IR because they are extremely sensitive. In addition, the probability of encountering an interfering signal is lower as long as UV detectors are shaded from sun light. Their drawbacks are the cost and their reduced efficiency with liquid hydrogen flames as fog blocks UV rays. The same remark applies whenever fog is present. False alarms can be released by random UV sources such as lightening or arc welding. The ability of the detector to discriminate sunlight induced UV radiation from hydrogen flames to avoid false alarms is the main challenge. Various techniques can be applied:

- The use of a filter to cut any wavelength above 0.29 µm to keep those wavelengths attributable only to a hydrogen fire accident. Indeed, even on a sunny day, the atmosphere filters sunray wavelengths below the proposed threshold of 0.29 µm. As a drawback, this solution also cuts down nearly 2/3 of the UV band and therefore decreases the detector accuracy.

- The use of two concomitant cells that watch the same zone. One of the cells mostly analyses the visible spectrum where the sunlight signal is predominant in comparison with hydrogen flame emitted signal whereas the other one focuses on the UV band. The UV signal from the UV cell is only taken into account if it diverges from the signal from the concomitant cell.
- The flickering behavior of a flame can also be considered. In that case, the modulated part of the UV signal would be looked at. This technique may not be compatible with a fast response need.
- Finally, if parasitic signals are known to be minor, a positive signal may be assumed whenever a given threshold is reached.

8.1.2 IR detectors

It has been mentioned how fog may hinder UV transmission to the sensor cell. IR detectors are not sensitive to these issues. Besides, hydrogen flames emit significant IR to use them for hydrogen flame detection. The main challenge remains the same as before to discriminate IR related to hydrogen fire from those of the sun, any light sources, or any hot materials. IR sources powered with alternative electric currents can be filtered due to their own 100 Hz modulated signal. However, neither hot bodies nor sunlight display a modulated signal that can be picked up and filtered.

The solution consists in focusing on the 1.7 µm wavelength that corresponds to a peak emission of steam.

8.1.3 Thermal detectors

Thermal detectors, e.g. temperature sensors, detect the heat of the flame. Thermal detectors work as rate-of-temperature-rise or overheat devices to pick up radiative, convective or conductive heat. These reliable detectors of various types are suitable hydrogen fire detection means as long as they are located very near where the fire breaks out. Such detectors need to be located very close to or at the site of a fire and are not specific to hydrogen flames.

8.1.4 Imaging systems

Imaging systems mainly are available in the thermal IR region and do not provide continuous monitoring with alarm capability. A trained operator is required to interpret whether the image being viewed is a flame. UV imaging systems require special optics and are very expensive.

Other common fire detectors type like those with ionising cells are not appropriate to detect hydrogen fires.

8.2 Mitigation of hydrogen fires

8.2.1 Control of the jet flow direction

The direction of hydrogen jet shall be oriented in such way that it does not reach people or equipment. For instance, flanges (i.e. components where hydrogen leaks are likely to occur)

should be positioned and directed in such way that a possible leak would not cause any domino effect.

8.2.2 Shielding or barriers

The main idea here is to reduce the rate of heat transfer to the potential targets in the vicinity of a hydrogen jet fire. The effect of barriers and walls was discussed earlier in this lecture. Flame shields are specifically designed to reduce the incident radiant heat flux by preventing direct flame impingement on equipment, structures and environment. The selection of materials, thickness, pressure and thermal effects for flame shields are very important.

8.2.3 Reduction of flame length

The approaches to reduce the flame length are:

- Minimise pipe diameters. It is clear from the analysis on jet fires that the flame length and jet extent are dependent on leak diameter. If pipe diameters cannot practically be made smaller, then consider inclusion of restrictors (see below).
- Minimise the pressure, i.e. if a system operates well at 0.2 bar, then supply hydrogen at the minimum value.
- Minimise the inventory of hydrogen in the system.
- Barrier walls can be used as a mitigation measure.
- Avoid positioning storage/PRDs/potential leak locations in the vicinity of the floor or a wall, as it may lead to a jet attachment and increase of a flammable jet or a jet fire.

Use of flow restrictors:

To reduce the flame length and therefore the hazard distance in case of unscheduled ignited hydrogen leak (fire) the use of flow restrictors in hydrogen supply lines is required. The feed line pressure, diameter of a pipe and restrictor orifice should, by design, limit the mass flow rate of hydrogen to a technological level that is required for the hydrogen system to function. Minimising pipe diameter would reduce flame length for potential pipeline full bore rupture at any location from the high-pressure storage.

A flow restrictor is commonly located immediately downstream of high-pressure storage to the pipeline [51]. Table 7 shows the effect of restrictor on the flame length from the pipe in assumption that restrictor is at some distance from the ruptured pipe (full bore rupture) exit. The flame would be even shorter if the pipe ruptured immediately after the restrictor (in this case reduction of flame length is proportional to reduction of diameter, i.e. ratio of pipe and restrictor diameter).

The general rule applied for the selection of the flow restrictor is as follows:

$$\frac{L_F^{no\ restriction}}{L_F^{restrictor}} = \left(\frac{D_F^{no\ restriction}}{D_F^{restrictor}} \right)^{2/3} \quad (17)$$

Table 7. The effect of a flow restrictor on flame length [51].

Storage pressure (bar)	Diameter (mm)	Restrictor diameter (mm)	Mass flow rate (kg/s)	Lf (m)
200	5	none	0.2282599	7.2398781
200	5	1	0.0091304	2.3694419
250	25	none	7.0009354	41.511453
250	25	1	0.0112015	4.4462877
350	5	none	0.3780851	8.6254101
350	5	1	0.0151234	2.822894
350	5	2	0.0604936	4.5667726
450	8	none	1.2018387	15.166747
450	8	1	0.0187787	3.5821849
450	10	none	1.877873	19.132678
450	10	1	0.0187787	3.8705775
450	10	2	0.0751149	6.2616759
450	15	none	4.2252142	29.180099
450	15	1	0.0187787	4.4553255
700	10	none	2.6929877	21.682279
700	10	1	0.0269299	4.3863665
700	10	2	0.1077195	7.0961002
700	25	none	16.831172	56.280825
700	25	1	0.0269299	6.0282339

Thermal activated pressure relief devices (TPRDs):

A new generation of TPRDs or safety valves can also be a very effective measure in reducing the flame length. Work is ongoing at Ulster University to improve the existing design of TPRDs as a mitigation device. Innovative PRDs will significantly decrease the flame length of hydrogen jet fires from current 10 m and more to about 1 - 2 m.

Recently, Yamazaki and Tamura [52] developed a simple method of verifying TPRD activation at post-fire accident sites. The verification technique is based on the measurement of hydrogen concentration at the TPRD gas release port, using a hydrogen densitometer. It was found that with the aid of a contact burning hydrogen densitometer, hydrogen concentrations exceeding 3,000 ppm could be measured continuously for about a month for Type III tanks and for about 24 hours for Type IV cylinders, even under the hostile test conditions of a vehicle burn-down fire accident [52].

8.2.4 Flashback and flame arrestors

A flash back arrestor is a safety device that shuts off gas flow in event of flash back. Flashback is the combustion of a flame mixture that can occur within a gas management system. This can

travel back through the line of gas management system to gas source if a flash back arrestor is not in line. A flash back arrestor shuts off gas flow and extinguishes the flame before it can reach the gas source. Flame arrestors are safety devices that allow flow of combustible gases while preventing ignition. The flame arrestor prevents the flame from transferring to a different area of a device by cooling or quenching a flame front or dampening a combustion wave. It is designed to absorb and dissipate the heat of a flame for specific operating and flow conditions.

A flame arrester, or flame trap, is a device used to prevent the passage of a flame along a pipe or duct. A flame arrester is generally an assembly of narrow passages, through which gas or vapour can flow, but which are too small to allow the passage of flame. Flame arresters are generally distinguished as end-of-line or in-line arresters [8].

There are three types of arresters [8]:

- Type 1 – arresters with multiple small channels (planar sheet metal, crimped ribbon, wire gauze, perforated plate, perforated block, sintered metal, parallel plate, wire pack, packed bed);
- Type 2 – hydraulic devices;
- Type 3 – velocity flame stoppers.

The operation of type 1 arresters is generally treated in terms of the mechanism of quenching and heat loss. Desirable properties of a flame arrester are high free cross-sectional area available for flow, low resistance to flow and freedom from blockage; a high capacity to absorb the heat of the flame, and the ability to withstand mechanical shock, including explosion. The design of flame arrester depends on the combustion properties of the flammable mixture and on the function and location of the arrester [8].

The size of the aperture through the arrester is determined by the quenching distance of the flammable mixture. The diameter of the aperture of an arrester should be smaller than the quenching diameter by at least 50%. The performance of an arrester is affected by the temperature. The quenching distance increases as the temperature increases. It is approx. inversely proportional to the square root of the absolute temperature. Hydraulic or liquid seal, arresters contain a liquid, usually water, which serves to break up the gas stream into bubbles and so prevents passage of the flame [8].

Velocity flame stoppers are arresters used in end-of-line applications. Their function is to prevent a flame passing from downstream to the upstream side. The principle of their operation is to assure that the velocity of the upstream gas passing through the arrester is sufficiently high to prevent a flame propagating through the arrester from the downstream side [8].

8.2.5 Use of thermal insulation

The basic purpose of thermal insulation is to reduce the rate of heat transfer to the potential targets, e.g. hydrogen tanks, in the vicinity of a hydrogen jet fire. Thermal insulation is achieved

by surrounding equipment with the materials that preferably have the following main characteristics:

- Relatively low thermal conductivity,
- Non-combustibility and the added attribute of not generating smoke or toxic gases when subjected to elevated temperatures,
- Product reliability giving positive assurance of consistent uniform protection characteristics,
- Availability in a form that permits efficient and uniform application,
- Sufficient bond strength and durability,
- Resistance to weathering or erosion resulting from atmospheric conditions.

Fire protection coatings (intumescent materials) providing thermal insulation can be a part of the fire protection strategy of compressed gaseous hydrogen vessels [21].

8.3 Extinction of hydrogen fires

The recommendations from the US National Hydrogen and Fuel Cell Emergency Response Training, 2014 are given below.

Responders should:

- listen for venting gas, and watch for thermal waves that would signal hydrogen flames;
- if only one FC vehicle is involved, approach from a 45° angle per standard procedures, and from a downhill and upwind position;
- if a hydrogen fire is present:
  - allow the hydrogen supply to burn out if safe to do so and protect adjacent exposures; then approach and extinguish;
  - if a hydrocarbon fire is also present, attack the fire with a straight water stream from a distance, but avoid directing the water stream into the hydrogen tank's pressure-relief-device vent line. Control fire spread and cool exposures;
  - if possible, direct venting hydrogen that is not burning away from ignition sources and dissipate if necessary with fog nozzle streams;
  - spray foam on petrol or diesel leaks near FC vehicle [53].

9. Flame length calculation of under-expanded jet fire

The thermal hazards of an under-expanded hydrogen jet fire released from a damaged pressurised storage system or TPRD opening was numerically studied by Cirrone et al. [54] at Ulster University. The simulation results were compared with the flame length and radiative heat flux measured for the horizontal jet fire experiment conducted at INERIS in France. The

model is based on the Reynolds-Averaged Navier-Stokes (RANS) conservation equations of mass, momentum, energy and species. Realizable k-ε model was used for turbulence modelling owing to its better capability of predicting the spreading rate of axisymmetric jets [55].

The release from the high-pressure hydrogen storage (930 bar) results in an under-expanded jet. The area, where the flow expands to ambient pressure, is characterised by the presence of shock waves and supersonic velocities, preventing the use of incompressible codes and requiring highly refined numerical grids. Therefore, the release source was modelled through the Ulster notional nozzle approach [1]. The model is based on mass and energy conservation equations, accounts the non-ideal behavior of hydrogen at extremely high pressure through the Abel-Noble equation of state, and describes the expansion process as isentropic. The flow is characterized by uniform sonic velocity and ambient pressure at the notional nozzle, simplifying significantly the problem by allowing to skip simulation of shock structures and considering the jet flow at the notional nozzle as completely expanded. Complete description of the approach and employed equations are available in Ref. [1].

Figure 39 shows the detail of the recess area and locations of five sensors measuring the radiative heat flux from the flame. The radiometers were located on a line forming a 45° angle with jet axis. The flame length was measured through a video camera positioned at 5 m distance from the flame. The tank temperature and pressure were recorded during the entire release duration.

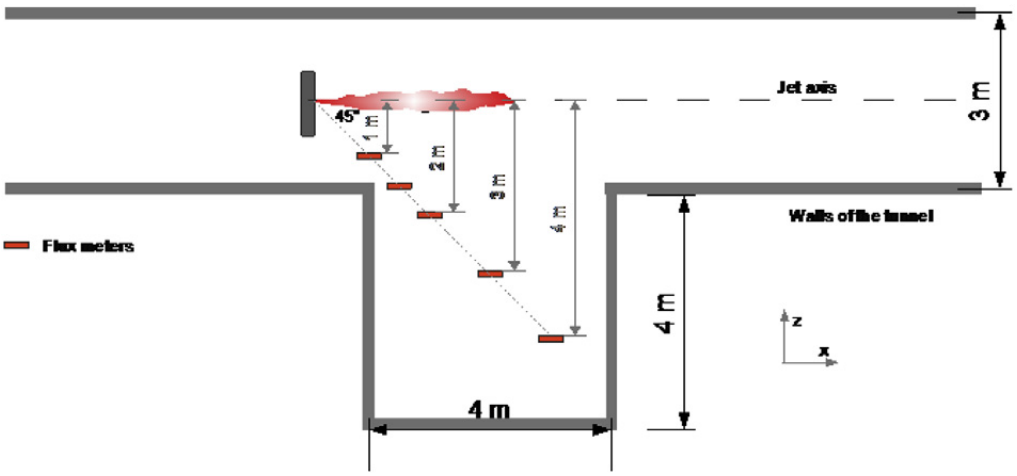

Figure 39. Details of recess area and sensor position [54].

The simulated flame length was calculated as the region of the flame characterised by range of temperature 1300-1500 K, according to the experimental observations on visible flame length made in Ref. [56]. The resulting flame length is represented by red bars in Figure 40, where simulations are compared to the experimental measurements made through a video camera. Flame length is well reproduced for a wide range of pressure decay in the tank, whereas it is over-predicted during the final phase of the release ($p < 200$ bar).

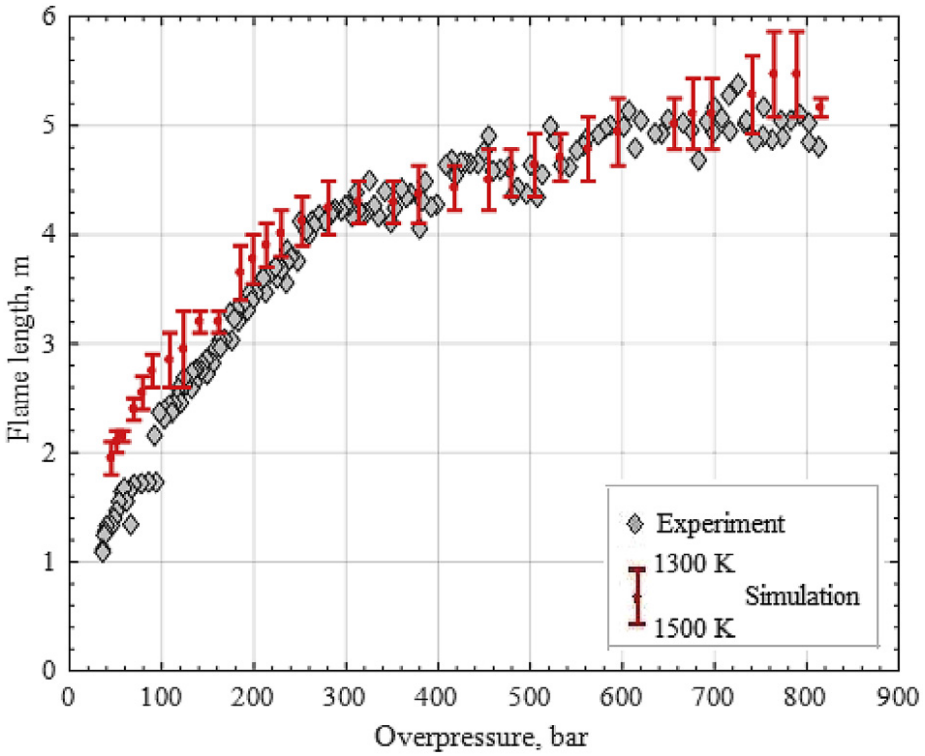

Figure 40. Flame lengths obtained by simulation and experiment [54].

Figure 41 shows the comparison between the experimental radiative heat fluxes (solid lines) and the simulated ones (dashed lines). The numeration of the sensors denotes the distance from the jet axis. During the first 10 s and except for sensor 1, simulation misrepresents the experimental radiative heat flux dynamics, resulting in significant underestimation. The dissimilarity may be attributed to both physical and numerical factors.

- First of all, the sudden release and combustion of the high-pressure hydrogen may cause the movement and entrainment of dust or other particles present on the gallery ground, which would affect the emitting volume and radiation intensity.
- Secondly, the exact location of the niche where the sensors are placed is not known. Position of the niche walls with respect to the jet affects exposure of sensors to the entire flame length with consequences on the detected radiative heat flux, especially for sensors 3 and 4.
- Furthermore, experimental observations on ignition of high-pressure gas releases shown a spherical broadening of the jet fire head during the first stage of the release (0-400 ms). This dynamics and flame stages were not detected in simulation.

Albeit the radiative heat flux discrepancies during the first phase of the release (about 10 s), the second phase showed a better agreement between the experimental and simulated thermal radiation fluxes. In spite of close agreement between the experimental and simulated flame lengths, modelling of radiative heat flux had a twofold limited predictive capability during the first stage of hydrogen release (t = 0-10 s) and quite a good agreement at later stage (t = 10-35

s). This may suggest that the experimental radiation was affected by some physical processes not unaccounted in CFD model, e.g. entrainment in jet flame and radiation of dust. However, the first stage of the release results to be the most dangerous, as it is characterized by the highest thermal radiation and flame length. It is therefore of primary importance to perform further numerical investigations to obtain better reproduction of experiment.

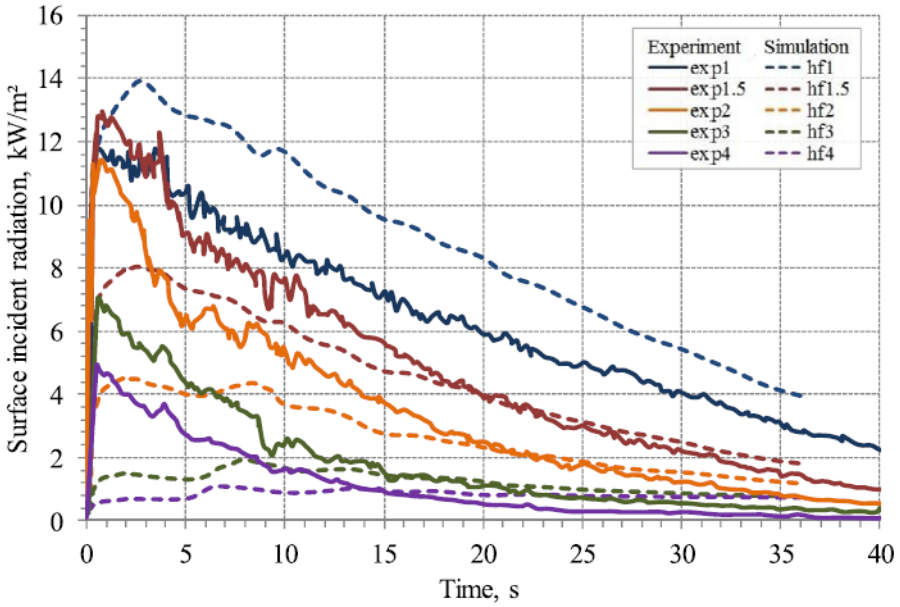

Figure 41. Radiative heat fluxes obtained by simulation and experiment [54].

10. Relevant e-Laboratory tools

10.1 Calculation of flame length

The model utilises a dimensionless flame length correlation described by Molkov & Saffers [25] for laminar and turbulent flames, buoyancy- and momentum-controlled fires, expanded (subsonic and sonic) and under-expanded (sonic and supersonic) jet fires, thereby covering the entire spectrum of hydrogen reacting leaks. The theory has been given in detail in section 3.3.2. The only dependence of the dimensionless flame length, L_F/D, is on parameters at the nozzle exit and on the density of the surrounding air. These parameters are density, ρ_N, and velocity, U_N, at the nozzle exit. Density and velocity can be normalized as ρ_N/ρ_S and U_N/C_N, respectively. Using the assumption that the kinetic energy flux in the nozzle exit is a conserved scalar of the process, a relationship between the density and the velocity in the dimensional group is introduced as $(\rho_N/\rho_S)\cdot(U_N/C_N)^3$, as shown in equation (6). This dimensionless hydrogen flame length correlation is shown in Figure 12.

Using this correlation it can be concluded:

- For subsonic flows (where M < 1) the dimensionless flame length depends on the nozzle Mach number only, as the density ratio ρ_N/ρ_S is practically constant for expanded jets.

- For choked flows (where M = 1) the dimensionless flame length depends only on the hydrogen density in the nozzle exit, ρ_N. Density increases with an increase in storage pressure and decrease in temperature.

The dimensionless correlation is validated within the following limits:

- In the range of hydrogen storage pressures from nearly atmospheric up to 900 bar,
- At temperatures down to 80 K, and
- In the range of nozzle diameters from 0.4 to 51.7 mm.

The hydrogen flow parameters presented in Figure 12 are either taken directly from experiments (dimensionless flame length, L_F/D) or calculated using under-expanded jet theory (density, flow rate, and speed of sound in the nozzle exit) following Molkov et al. [57]. Details of the experimental data utilised is described in Molkov and Saffers [58].

When utilising the tool of e-Laboratory to calculate the flame length (https://elab-prod.iket.kit.edu/), the tool – *Flame length correlation and three hazard distances for jet fires* – should be selected. As shown in Figure 42, the input parameters include hydrogen pressure in reservoir p_1, hydrogen temperature in reservoir T_1, orifice diameter d_3, ambient pressure p_4 and ambient temperature T_{atm}, respectively.

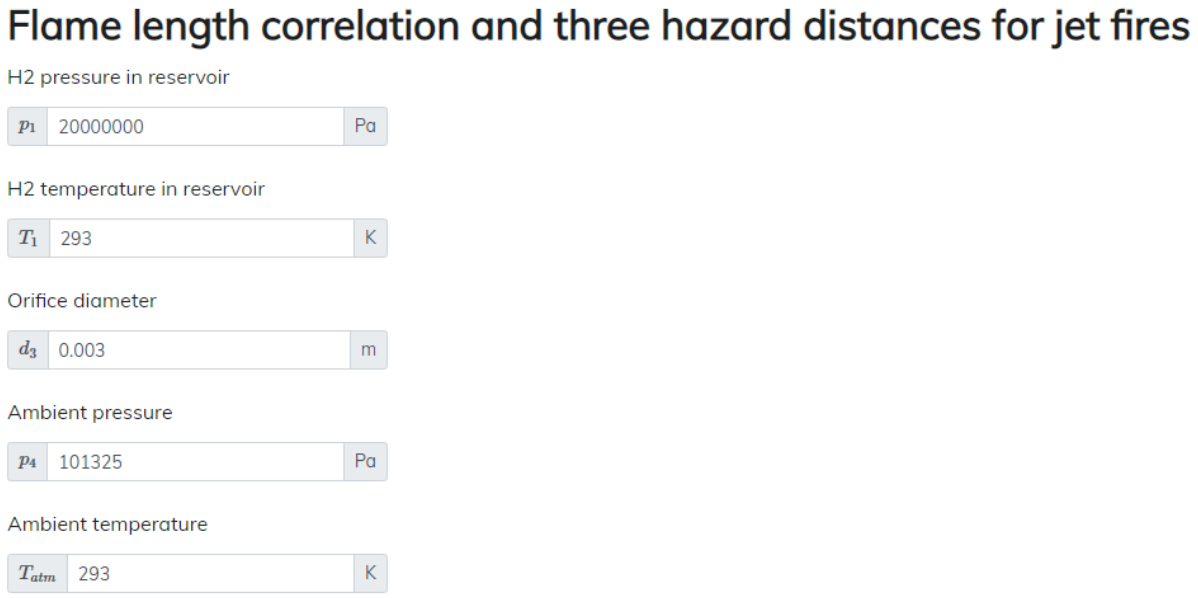

Figure 42 Input parameters of the tool of flame length correlation and three hazard distances for jet fires

After calculation, the flame length and three different hazard distances are obtained. An example of the output parameters is given in Figure 43.

Flame length correlation and three hazard distances for jet fires

Name	Symbol	Value	Unit
H2 pressure in reservoir	p_1	2e+7	Pa
H2 temperature in reservoir	T_1	293	K
Orifice diameter	d_3	0.003	m
Ambient pressure	p_4	1.01325e+5	Pa
Ambient temperature	T_{atm}	293	K
Flame length	L_F	6.259	m

Figure 43 Output parameters of the tool of flame length correlation and three hazard distances for jet fires.

The calculated flame lengths as a function of TPRD diameter in few typical cases are shown in Table 8.

Table 8 Calculated flame length vs. TPRD diameter in typical cases

Storage pressure (bar)	Orifice diameter (mm)	Tank temperature (°C)	Flame length (m)
350	1.0	20	2.6
700	1.0	20	3.3
350	1.0	50	2.5
700	1.0	50	3.2
350	3.0	20	7.8
700	3.0	20	9.9
350	3.0	50	7.5
700	3.0	50	9.6
350	1.0	100	3.1
700	3.0	100	9.2

10.2 Expanded and under-expanded jet

The theory of under-expanded and expanded jet has been showed in Lecture 7 – Unignited hydrogen releases outdoors and their mitigation. Basically, the critical pressure ratio across the leak, p^*, determines whether the flow is subsonic or sonic /supersonic.

$$p^* = \frac{p_1}{p_{atm}} = \left[\frac{(\gamma+1)}{2}\right]^{\gamma/(\gamma-1)} \quad (16)$$

Therefore, the critical pressure ratio for the transition to sonic flow for hydrogen is ≈ 1.9. If p^* < 1.9, the flow is subsonic and expanded, as long as p^* > 1.9, the exit velocity remains locally sonic and the jet is under-expanded. The exit pressure rises above ambient with the result that expansion, down to ambient pressure, p_{atm}, takes place outside of the real nozzle at a location downstream of the Mach disc, called the effective nozzle diameter.

Therefore, different equation sets must be solved depending on whether the flow is expanded or under-expanded, the equation set relating to an under-expanded jet is detailed in Ref. [1].

When utilising the tool of e-Laboratory to calculate the expanded and under-expanded jet, the tool – *Similarity law for concentration decay in hydrogen expanded and under-expanded jets and unignited jet hazard distances* – should be selected. The input parameters are same as those in Figure 42. After calculation, the axial distance from nozzle with respect to different hydrogen concentrations are obtained. An example of the output parameters is given in Figure 44.

Similarity law for concentration decay in hydrogen expanded and under-expanded jets and unignited jet hazard distances

Name	Symbol	Value	Unit
H2 pressure in reservoir	p_1	3.5e+7	Pa
H2 temperature in reservoir	T_1	293	K
Orifice diameter	d_3	0.005	m
Ambient pressure	p_4	1.01325e+5	Pa
Ambient temperature	T_{atm}	293	K
Axial distance from nozzle to 4% by vol. H2	$X_{4\%,H_2}$	32.6212	m
Axial distance from nozzle to 8% by vol. H2	$X_{8\%,H_2}$	15.6793	m
Axial distance from nozzle to 11% by vol. H2	$X_{11\%,H_2}$	11.0593	m
Axial distance from nozzle to 16% by vol. H2	$X_{16\%,H_2}$	7.20885	m
Axial distance from nozzle to 29.5% by vol. H2	$X_{29.5\%,H_2}$	3.33269	m

Figure 44 Output parameters of the tool of similarity law for concentration decay in hydrogen expanded and under-expanded jets and unignited jet hazard distances.

10.3 Calculation of hazard distance

Following release, jets can be divided into three types: fully momentum-dominated, transitional and fully buoyancy-dominated, which has been described in detail in Lecture 7 – Unignited hydrogen releases outdoors and their mitigation. Fully momentum-dominated jets are not affected by buoyancy whereas fully buoyancy-dominated jets are quickly diverted from the horizontal to vertical flow direction. Transitional jets are initially momentum-dominated close to the nozzle and then further downstream, as velocity drops and jet diameter increases, they become buoyancy-dominated. When considering hydrogen safety engineering it is important to know when this transition takes place, as it has direct consequences for the required separation distance to maintain safety.

Using the flame length calculations performed, the required hazard distance when considering momentum dominated straight flames for each of the criteria listed below can be calculated.

So called "harm criteria" for people can be expressed in terms of injury or death [59].

These criteria can be written as follows:

- No harm limit, 70 °C: $x = 3.5 \times L_F$
- Pain limit for 5 min exposure, 115 °C: $x = 3.0 \times L_F$
- Third degree burns (20 s), 309 °C: $x = 2.0 \times L_F$

It should be noted that the authors have selected the "harm criteria" from LaChance [59] as a basis for the calculation of separation distance for demonstration purposes only. A universally accepted standard for this calculation has not yet been agreed at National, European or International level.

When utilising the tool of e-Laboratory to calculate three hazard distances for jet fires, the tool – *Flame length correlation and three hazard distances for jet fires* – should be selected. The input parameters are same as those in Figure 42. After calculation, the flame length and three hazard distances (no harm, pain limit, and third-degree burns) are obtained. An example of the output parameters is given in Figure 45.

Flame length correlation and three hazard distances for jet fires

Name	Symbol	Value	Unit
H2 pressure in reservoir	p_1	2e+7	Pa
H2 temperature in reservoir	T_1	293	K
Orifice diameter	d_3	0.003	m
Ambient pressure	p_4	1.01325e+5	Pa
Ambient temperature	T_{atm}	293	K
Flame length	L_F	6.259	m
No harm (70°C) separation distance	X_{70}	21.9065	m
Pain limit (5 mins, 115°C) separation distance	X_{115}	18.777	m
Third degree burns (20 sec, 309°C) separation distance	X_{309}	12.518	m

Figure 45 Output parameters of the tool of flame length correlation and three hazard distances for jet fires.

Acknowledgement

The HyResponse project is acknowledged as the materials presented here are extended based on the original HyResponse lectures.

References

1. Molkov, V (2012). Fundamentals of hydrogen safety engineering, Part I and Part II. Available from: www.bookboon.com, free download e-book.

2. Cheng, TS, Chiou, CR (1998). Experimental investigation of the characteristics of turbulent hydrogen jet flames. Combustion Science and Technology. Col. 136, p. 81-84.
3. Dorofeev, SB (2009). Evaluation of hydrogen explosion hazards: phenomenology and potential flame acceleration and DDT. 4th European Summer School on Hydrogen Safety.
4. Birch, AD, Brown, MG, Dodson, MG, Swaffield, F (1984). The structure and concentration decay of high pressure jets of natural gas. Combustion Science and Technology. Vol. 36, p. 249-261.
5. NFPA®52. Vehicular Natural Gas Fuel Systems Code, 2019 Edition.
6. LaChance, J, Tchouvelev, A and Engebo, A (2011). Development of uniform harm criteria for use in quantitative risk analysis of the hydrogen infrastructure. International Journal of Hydrogen Energy. Vol. 36 p. 2381-2388.
7. Saffers, JB (2010). Principles of hydrogen safety engineering. PhD thesis. University of Ulster.
8. BRHS, Biannual Report on Hydrogen Safety (2007). Network of Excellence HySAFE. Available from: http://www.hysafe.org/BRHS [accessed on 25.11.20].
9. Kanury, AM (1975). Introduction to combustion phenomena: (for fire, incineration, pollution and energy applications). New York; London: Gordon and Breach.
10. Teodorczyk, A (2006). Fast deflagration, deflagration to detonation transition (DDT) and direct detonation of hydrogen-air mixtures. Teaching Materials of European Summer School on Hydrogen Safety, 2006.
11. Kalghatgi, GT (1981). Blow-out stability of gaseous jet diffusion flames. Part I: in still air. Combustion Science and Technology. Vol. 26(5), pp. 233-239.
12. Matta, LM, Neumeier, Y, Lemon, B and Zinn, BT (2002). Characteristics of microscale diffusion flames. *Proceedings of the Combustion Institute*, vol. 29, pp. 933-938.
13. Cheng, TS, Chen, CP, Chen, CS, Li, YH, Wu, CY and Chao, YC (2006). Characteristics of microjet methane diffusion flames. *Combustion Theory and Modelling*, 10, pp. 861-881.
14. Butler, MS, Moran, CW, Suderland, PB and Axelbaum, RL (2009). Limits for hydrogen leaks that can support stable flames. International Journal of Hydrogen Energy. Vol. 34. pp. 5174-5182.
15. Sunderland, PB (2010). Hydrogen microflame hazards, Proceedings of the 8th International Short Course and Advanced Research Workshop in the series “Progress in Hydrogen Safety”, Hydrogen and Fuel Cell Early Market Applications, 11 - 15 October 2010, University of Ulster, Belfast.

16. Hawthorne, WR, Weddell, DS and Hottel HC (1949). Mixing and combustion in turbulent gas jets, Third International Symposium on Combustion, Flame and Explosion Phenomena, pp. 266-288, Baltimore, USA.

17. Hottel, HC and Hawthorne, WR (1949). Diffusion in laminar flame jets. Proceedings of the Combustion Institute. Vol. 3, pp. 254-266.

18. Brennan, S, Makarov, D and Molkov, V (2009). LES of high pressure hydrogen jet fire. Journal of Loss Prevention in the Process Industries. Vol. 22 (3), pp.353-359.

19. Baev, VK and Yasakov, VA (1974). Effect of lifting forces on the length of diffusion flames. Combustion, Explosion and Shock Waves. Vol. 10, pp. 752-758.

20. Shevyakov, GG and Komov, VF (1977). Effect of non-combustible admixtures on length of an axisymmetric on-port turbulent diffusion flame. Combustion, Explosion and Shock Waves. Vol. 13, pp. 563-566.

21. HyFacts Project. Chapter F. Hydrogen fires. Available from: https://www.h2euro.org/hyfacts/2014/06/26/training-material/ [accessed on 25.11.20].

22. Kalghatgi, GT (1984). Lift-off heights and visible lengths of vertical turbulent jet diffusion flames in still air. Combustion Science and Technology. Vol. 41, pp. 17-29.

23. Schefer, RW, Houf, WG, Bourne, B and Colton, J (2006). Spatial and radiative properties of an open-flame hydrogen plume. International Journal of Hydrogen Energy. Vol. 31, pp. 1332-1340.

24. Schefer, RW, Houf, WG, Williams, TC, Bourne, B and Colton, J (2007). Characterization of high pressure, underexpanded hydrogen-jet flames. International Journal of Hydrogen Energy. Vol. 32, pp. 2081-2093.

25. Molkov, V and Saffers, J-B (2013). Hydrogen jet flames. International Journal of Hydrogen Energy. Vol. 38, pp. 8141-8158.

26. Proust, C, Jamois, D and Studer, E (2009). High pressure hydrogen fires. *Proceedings of the Third International Conference on Hydrogen Safety*. 16-18 September 2009, Ajaccio, France, paper 214.

27. LaChance, J, Tchouvelev, A and Engebo, A (2011). Development of uniform harm criteria for use in quantitative risk analysis of the hydrogen infrastructure. International Journal of Hydrogen Energy. Vol. 36 pp. 2381-2388.

28. EIGA, European Industrial Gases Association (2007). Determination of safety distances. IGC Doc 75/07/E.

29. BSI British Standards Institution (2004). Published Document PD 7974-6:2004. The application of fire safety engineering principles to fire safety design of buildings - Part 6:

Human factors: Life safety strategies - Occupants evacuation, behaviour and condition (Sub-system 6).

30. DNV Technica (2001). Human resistance against thermal effects, explosion effects, toxic effects and obscuration of vision. DNV Technica, Scandpower A/S, Det Norske Veritas, Oslo, Norway.
31. BSI British Standards Institution (1997). British Standard 7899:1997. Code of practice for assessment of hazard to life and health from fire. Guidance on methods for the quantification of hazards to life and health and estimation of time to incapacitation and death in fires.
32. Barlow, RS and Carter, CD (1996.) Relationships among Nitric Oxide, Temperature, and Mixture Fraction in Hydrogen Jet Flames. Combustion and Flame. Vol. 104, pp. 288-299.
33. Imamura, T, Hamada, S, Mogi, T, Wada, Y, Horiguchi, S, Miyake, A and Ogawa, T (2008). Experimental investigation on the thermal properties of hydrogen jet flame and hot currents in the downstream region. International Journal of Hydrogen Energy. Vol. 33, pp. 3426-3435.
34. Royle, M and Willoughby, DB (2009). Consequences of catastrophic releases of ignited and unignited hydrogen jet releases. 3rd International Conference on Hydrogen Safety, Ajaccio, France.
35. Mogi, T and Horiguchi, S (2009). Experimental study on the hazards of high-pressure hydrogen jet diffusion flames. Journal of Loss Prevention in the Process Industries. Vol. 22, pp. 45-51.
36. Makarov, D and Molkov, V. (2013). Plane hydrogen jets. International Journal of Hydrogen Energy. Vol. 38 (19), pp. 8068–8083.
37. Shevyakov, GG and Savelieva, NI (2004). Dispersion and combustion of hydrogen jet in the open atmosphere. International Scientific Journal for Alternative Energy and Ecology. Vol. 1(9), pp. 23-27 (in Russian).
38. HYPER (2008) FP6 STREP project “Installation Permitting Guidance for Hydrogen and Fuel Cells Stationary Applications”. *Deliverable 4.3 Releases, Fires and Explosions*. WP4 Final Report.
39. Houf, WG and Schefer, RW (2007). Predicting radiative heat fluxes and flammability envelopes from unintended releases of hydrogen. International Journal of Hydrogen Energy. Vol. 32, pp. 136-151.
40. Molina, A, Schefer, RW and Houf, WG (2007). Radiative fraction and optical thickness in large-scale hydrogen-jet fires. Proceedings of the Combustion Institute. Vol. 31, pp. 2565-2572.

41. Case for safety. Relative frequency of failure modes. Available from: http://h2safe.net/case_safety.html [accessed on 25.11.20].

42. Zalosh, R (2007). Blast waves and fireballs generated by hydrogen fuel tank rupture during fire exposure. Proceedings on the 5th Seminar on Fire and Explosion Hazard, Edinburgh, UK, 23-27 April 2007, pp. 2154-2161.

43. Fire statistics, Great Britain, 2011-2012. Department of Communities and Local Government.

44. Gambone, LR and Wong, JY (2007). Fire protection strategy for compressed hydrogen-powered vehicles. 2nd International Conference on Hydrogen Safety, San Sebastian, Spain, 11-13 September, 2007.

45. Swain, MR (2001). Fuel leak simulation. Proceedings of the 2001 DOE Hydrogen Program Review. Available from: https://www1.eere.energy.gov/hydrogenandfuelcells/pdfs/30535be.pdf [Accessed 25.11.20].

46. Tamura, Y, Takabayashi, M, Takeuchi, M and Mitsuishi, H (2011). The spread of fire from adjoining vehicles to a hydrogen fuel cell vehicle. In: Proceedings of the Fourth International Conference on Hydrogen Safety, 12-14 September 2011, San Francisco, USA.

47. Stephenson, RR (2005) Fire safety of hydrogen-fuelled vehicles: system-level bonfire test. Proceedings of the 1st International Conference on Hydrogen Safety, Pisa, Italy, 2005. Available from: http://conference.ing.unipi.it/ichs2005. [Accessed 25.11.20].

48. Watanabe, S, Tamura, Y, Suzuki, J (2007). The new facility for hydrogen and fuel cell vehicle safety evaluation. International Journal of Hydrogen Energy. Vol. 32 (13), pp. 2154-2161.

49. Li, Z, Makarov, D, Keenan, J, Molkov, V (2015). CFD study of the unignited and ignited hydrogen releases from TPRD under a fuel cell car. 6th International Conference on Hydrogen Safety, 19-21 October 2015, Yokohama, Japan.

50. NFPA 1971, Standard on Protective Ensembles for Structural Fire Fighting and Proximity Fire Fighting, 2007 Edition. National Fire Prevention Association, 2007, Boston, Massachusetts.

51. HyIndoor Deliverable D4.2 – First intermediate report on analytical, numerical and experimental studies (2014).

52. Yamazaki, K and Tamura, Y (2015). Study of a Post-fire Verification Method for the Activation Status of Hydrogen Cylinder Pressure Relief Devices. 6th International Conference on Hydrogen Safety, 19-21 October 2015, Yokohama, Japan.

53. US DoE, US Department of Energy (2008). Hydrogen safety training for first responders. Available from: http://hydrogen.pnl.gov/FirstResponders/ [accessed on 25.11.20].

54. Cirrone DMC, Makarov D, Molkov V. Simulation of thermal hazards from hydrogen under-expanded jet fire. Int J Hydrogen Energy 2019,44:8886-8892.

55. ANSYS Fluent. Theory guide. 2016.

56. Schefer R, Houf B, Bourne B, Colton J. Experimental measurements to characterize the thermal and radiation properties of an open-flame hydrogen plume. In: Proceedings of the 15th annual hydrogen conference and hydrogen expo; 2004.

57. Molkov, V., Makarov, D. and Bragin, M., 'Physics and modeling of under-expanded jets and hydrogen dispersion in atmosphere', in Proceedings of the 24th International Conference on Interaction of Intense Energy Fluxes with Matter, 1st - 6th March, 2009, Elbrus, Russia, 2009, p. 146.

58. Molkov, V. and Saffers, J.-B., 'The correlation for non-premixed hydrogen jet flame length in still air', in 10th International Symposium on Fire Safety Science, June 19, 2011 - June 24, 2011, 2011, pp. 933–943.

59. LaChance, J.L., 'Progress in risk assessment methodologies for emerging hydrogen applications', presented at the Sixth International Short Course and Advanced Research Workshop 'Progress in Hydrogen Safety - Regulations, Codes and Standards' 25th - 29th January, 2010, Belfast, Northern Ireland, 2010.

60. Wang H., Duncan I.J. Likelihood, causes, and consequences of focused leakage and rupture of U.S. natural transmission pipelines. J. Loss Prevent. Proc. 2014, 30: 177-187.

61. U.S. Department of Tranportation. Pipeline and Hazardous Materials Safety Administration. (2010). https://primis.phmsa.dot.gov/comm/publications/PIPA/PIPA-PipelineRiskReport-Final-20101021.pdf

62. Lowesmith B.J., Hankinson G. Large scale high pressure jet fires involving natural gas and natural gas/hydrogen mixtures. Process Saf. Environ. 2012, 90: 108-120.

63. EGIG, Gas pipeline incidents 8th Report of the European Gas Pipeline Incident Data Group, EGIG 14.R.0403 (2011).

64. Casal J., Gomez-Mares M., Munoz M., Palacios A. Jet fires: a "minor" fire hazard? Chem. Eng. Trans. 2012, 26: 13-20.

65. Houf W., Schefer R. Predicting radiative heat fluxes and flammability envelopes from unintended releases of hydrogen. Int. J. Hydrogen Energy, 2007, 32: 136-151.

66. Lin CL, Chien CF. Systems thinking in a gas explosion accident e lessons learned from Taiwan. J Loss Prev Process Ind 2019, 62:103987.

67. EIGA. Determination of safety distances (IGC Doc 75/07/E). 2007. https://www.eiga.eu/publications/eiga-documents/doc-7507-determination-of-safety-distances/ [Accessed 12.02.2020].

68. Gomez-Mares M., Zarate L., Casal J. Jet fires and the domino effect. Fire Saf J. 2008, 43: 583-588.

69. Cirrone DMC, Makarov D, Molkov V. Simulation of thermal hazards from hydrogen under-expanded jet fire. Int J Hydrogen Energy 2019, 44: 8886-8892.

70. Wang Z, Shui K, You F, Dederichs AS, Markert F, Jiang J, Zhang Y, Li D, Fu Z, Xu J, He L, Huangfu W. Prediction of the failure probability of the overhead power line exposed to large-scale jet fires induced by high-pressure gas leakage. Int J Hydrogen Energy 2021, 46: 2413-2431.

71. Coccorullo I, Russo P. Jet fire consequence modeling for high-pressure gas pipelines, International conference of computational methods in sciences and engineering 2016 (iccmse 2016).

72. Molkov VV, Cirrone DMC, Shentsov VV, Dery W, Kim W, Makarov DV. Dynamics of blast wave and fireball after hydrogen tank rupture in a fire in the open atmosphere. Int J Hydrogen Energy, 2021, 46: 4644-4665.